Marine Geology 408 (2019) 123–143

Contents lists available at ScienceDirect

Marine Geology

journal homepage: www.elsevier.com/locate/margo

Impact of dense bottom water on a continental shelf: An example from the SW Adriatic margin

M. Rovere[a,*], C. Pellegrini[a], J. Chiggiato[b], E. Campiani[a], F. Trincardi[a]

[a] ISMAR CNR, Via P. Gobetti 101, 40129 Bologna, Italy
[b] ISMAR CNR, Arsenale - Tesa 104 Castello 2737/F, 30122 Venezia, Italy

ARTICLE INFO

Keywords:
Adriatic Sea
Continental shelf morphology
Sand dunes
Contourites
Dense Shelf Water

ABSTRACT

Dense shelf waters have been recognised as a key factor in transporting sediment and organic matter across continental slopes; however, the effect of their circulation on continental shelves is still overlooked. The Adriatic Sea is one of the areas in the Mediterranean where dense shelf water forms and flows as a bottom-hugging gravity current along the continental margin. A fraction of this dense water passes beyond the shelf break and flows downslope through cascading, while a large (lighter and faster) portion remains on the shelf, with a principal vein flowing between 80 and 120 m water depth.

This paper presents the 3D shape, internal architecture and sediment facies of a variety of large-scale sedimentary features detected on the continental shelf and at the shelf edge, between 50 and 300 m water depth. These features include giant comet marks, large flute-shaped scours, muddy sediment waves, very large dunes with superimposed bedforms, active and relict sand ridges and shelf edge contourites. Both erosional and depositional features show an overall internal geometry and orientation consistent with water masses flowing southward, and are located where flows become accelerated by topographic constraints and deviated by the curvature of the shelf edge.

In this study, the morphology and seismic stratigraphic structure of large-scale bedforms are investigated in an effort to place constraints on bedform evolution and preservation, especially as predictive tools for sand resource management, and to bring new evidence of the interaction between unidirectional hydrodynamic processes and seafloor dynamics on the shelf.

1. Introduction

Understanding the origin of sand deposits on modern outer continental shelves has always impinged on two interrelated problems: what was relative sea level at the time of formation of these deposits and what was the specific process or combination of processes leading to their formation and preservation. This long lasting discussion still refers to the classification proposed by Swift et al. (1971), which recognised relict, palimpsest (later called moribund, *e.g.,* Dyer and Huntley, 1999) and active sand deposits. The first are no longer active after drowning by sea level rise; the second are occasionally active in the presence of exceptional hydrodynamic events; the third are in equilibrium with present-day oceanographic processes and therefore continuously reworked by a regionally-variable combination of tides, storm waves and thermohaline currents. Shoreface-connected ridges, for example, are generated primarily by storm-driven longshore currents interacting with a rugged nearshore topography where drowned barrier islands or ebb-tidal deltas act as ridge precursors (Calvete et al., 2001; Dyer and Huntley, 1999; Guerrero et al., 2018; McBride and Moslow, 1991; Snedden et al., 2011; Swift et al., 1978). They detach from the coast during sea level rise (McBride and Moslow, 1991), through a phase of increase in height and asymmetry, and a progressive decrease of their migration speed (Nnafie et al., 2014).

Thus, intuitively, the deeper on the shelf such sandy deposits occur, the most likely is their relict or palimpsest nature. Noteworthy exceptions to this assumption come from areas impacted by geostrophic currents, such as the South African shelf (Flemming, 1980; Ramsay et al., 1996), the East Antarctica shelf (Harris et al., 2001), the southern Japanese margin (Kubo et al., 2004) or by the intrusion of thermohaline currents, like the Uruguayan margin (Hernández-Molina et al., 2016). Enforcement of unidirectional currents can be favored by topographic constrictions (Lo Iacono et al., 2010; Pellegrini et al., 2016). Therefore, the large-scale bedforms, located in the outer shelves, should not be regarded as solely relict sedimentary features with no or limited chance

* Corresponding author.
E-mail address: marzia.rovere@bo.ismar.cnr.it (M. Rovere).

https://doi.org/10.1016/j.margeo.2018.12.002
Received 9 July 2018; Received in revised form 4 November 2018; Accepted 4 December 2018
Available online 08 December 2018

of migration and preservation (Goff et al., 1999), but considered as integral part of the seafloor dynamics of the continental shelf. Understanding the mechanisms of transport, the quantity of material transported and predicting the potential dynamic behaviour of such large-scale bedforms is integral to proper resource management, because these are often preferred borrowing areas for the construction industry, land reclamation and beach nourishment projects.

Unidirectional flows, such as dense shelf waters, generated in shallow shelf areas through winter cooling, have been increasingly recognised as a key factor in sediment-transport across continental slopes (Canals et al., 2006); however, the impact of such water masses on continental shelves has received far less attention. An exception comes from the SW Adriatic Margin (SAM), in the Central Mediterranean Sea, which has been the subject of a wealth of studies on the flow of dense shelf water (Bignami et al., 1990; Chiggiato et al., 2016). Strong flows generated by cascading of the North Adriatic Dense Water (NAdDW) trigger intense off-shelf fluxes of water, sediment and particulate matter to deep-sea environments of the SAM (Langone et al., 2016; Pellegrini et al., 2016; Trincardi et al., 2007). Part of the dense water flow is documented to adjust and flow along the bathymetric contour of the SAM shelf. While this process has been extensively documented in physical oceanography, no studies of its potential interaction with the shelf seafloor have been put forward. This study aims at filling in this gap by providing evidence of the existence of bottom current-related bedforms, which mostly formed during the last postglacial sea level rise, but that can still be modified by unidirectional shelf dense waters, which in turn are accelerated by both the overall morphology of the margin and bathymetric changes, including the presence of seafloor obstacles. For this broader scope, we present new high-resolution geophysical and ground truth data, which cover almost the entire 250 km long shelf from offshore Gargano Promontory up to the southernmost tip of the Apulian Peninsula (Fig. 1). The integrated data set provides the first accurate overview of the SAM shelf morphology up to 5-m-grid resolution and showcases it as a paradigmatic case to predict where it is more likely to find bottom current-related deposits over the shelf and along the shelf edge.

2. Oceanographic setting

2.1. Tide, waves and currents

The continental shelf of the SAM is characterized by a microtidal regime with generally very weak tidal currents. Relatively speaking, the most intense values along the SAM are found in proximity of the Strait of Otranto (0.10–0.15 m s^{-1}), with dominant alongshore directions (Cushman-Roisin and Naimie, 2002; Fig. 2B). During the summer season with stratified water column, interaction of diurnal tides with the topography may intensify bottom currents near the shelf edge by an additional 10 cm s^{-1} (Ursella et al., 2014).

The wave climate is bimodal, according to decadal observations in Monopoli (1989–2001; Fig. 2A) from the national buoy network, with most frequent sea states coming from the north-west and secondarily east – southeast. Most intense sea state recorded was significant wave height (Hs) = 5.2 m and peak wave period (Tp) = 10 s (Piscopia et al., 2004). Close to Cape Otranto, the sea state is less fetch-limited, in particular from the south, thus slightly more severe sea states occur. A seven years (2010–2016) time series, built on wave model hindcast from Copernicus — Marine Environment Monitoring Service (CMEMS), show similar values in Hs and Tp, with longest Tp between 10 and 12 s (Fig. 2A). Applying the rule-of-thumb of wave base line as half the wavelength, the limit of wave action on the seafloor is 75 m (10 s) in the northern sector of the SAM and 110 m (12 s) in the southern sector of the SAM.

The overall circulation in the area is cyclonic (*i.e.* locally southeastward). Mooring data across the shelf during 1994–1995 recorded maximum bottom current intensities of some 0.5 m s^{-1} (water depth 120 m) and 0.4 m s^{-1} (shelf edge, water depth 132 m). These values come from unfiltered time series, thus including the mean flow as well as tidal and subtidal (mostly synoptic scale) fluctuations (Kovačević et al., 1999). Using simplified formulae, assuming a flat bed and current-only bottom boundary layer (*e.g.*, Madsen and Wood, 2002), velocities measured at mooring sites (15 m above the sea bottom) indicate that a large part of the SAM shelf is affected by a bottom shear stress between 0.1 and 0.2 N m^{-2}, with fine sands and exceptionally medium sands affected at least by resuspension (Fig. 2C).

The most important thermohaline currents are: the Western Adriatic Coastal Current (WACC), a coastal current originated as a geostrophic response of the river runoff mostly in the Northern Adriatic and travelling on the SAM shelf with an intensity of some 0.30 m s^{-1} (Poulain, 2001); shelf dense water currents (see Section 2.2) travelling on the outer shelf, during the spreading phase of dense water generated in the northern Adriatic shelf area.

2.2. Dense shelf water

The SAM is affected by distinct water masses that include the Levantine Intermediate Water (LIW) and the seasonally modulated North Adriatic Dense shelf Water (NAdDW) (Fig. 1; Artegiani et al., 1997). Both the LIW and the NAdDW are characterized by annual and interannual fluctuations in density, flow strength and sediment transport capacity (Turchetto et al., 2007). The NAdDW forms on the shallow northern Adriatic shelf (Fig. 1) and its density increases (up to 30 kg m^{-3}, Mihanović et al., 2013) by winter cooling and evaporation associated with dry and cold north-easterlies (Bora wind, *e.g.,* Dorman et al., 2007; Signell et al., 2010). The NAdDW formation is modulated seasonally with a typical occurrence in February–March, exhibiting a significant interannual variability in terms of volume and thermohaline properties in response to winter conditions. Advection of salinity from the southern Adriatic or freshwater discharge from rivers, during the preconditioning phase, eventually assist or limit the dense water production. Once formed, the NAdDW flows southward along the isobaths of the Italian continental shelf and slope, driven by its excess density as a bottom-hugging gravity current deflected rightwards by the Coriolis force (Vilibić and Supić, 2005). Oscillating around a geostrophic equilibrium under the effect of pulsing forcing, such as tidal, subtidal and inertial oscillations, the western part of the NAdDW flows nearly parallel to the western Adriatic coast at an average velocity of the order 0.10–0.30 m s^{-1} (Chiggiato et al., 2016), with strong variability. Occasionally, storm-induced pulses of kinetic energy cause the current speed on the shelf to rise > 0.40 m s^{-1} (Benetazzo et al., 2014). The gravity current travelling along the Italian shelf eventually reaches the southern Adriatic, where it sinks through successive cascading events. On the contrary, lighter and faster water masses continue to flow southwards along the shelf up to the Strait of Otranto where they become attenuated in density and velocity (Carniel et al., 2016). The fraction of dense water, which flows downslope with mean velocities around 0.3–0.4 m s^{-1} up to 0.8 m s^{-1} (Chiggiato et al., 2016), generates a variety of depositional and erosional sedimentary features and interacts with the slope morphology (Bonaldo et al., 2016; Foglini et al., 2016; Pellegrini et al., 2016; Verdicchio et al., 2007). After the exceptional event of winter 2012, the principal vein on the shelf was found between 80 and 120 m (Chiggiato et al., 2016), with instant velocities up to 0.25 m s^{-1}, while along the shelf edge, in specific sectors, numerical modelling experiments show current speed peaks above 0.70 m s^{-1} (Bonaldo et al., 2016).

This oceanographic regime can be extended into the past at least from the last post-glacial sea level rise. The formation of dense shelf water, in fact, is suggested to be inhibited during periods of sea level lowstand due to the concomitant North Adriatic shelf exposure and reduced cold Bora wind forcing (Pellegrini et al., 2016; Verdicchio and Trincardi, 2008). After the Last Glacial Maximum, the unidirectional current became reactivated *ca.* 11.5 kyr BP, as suggested by along-shelf

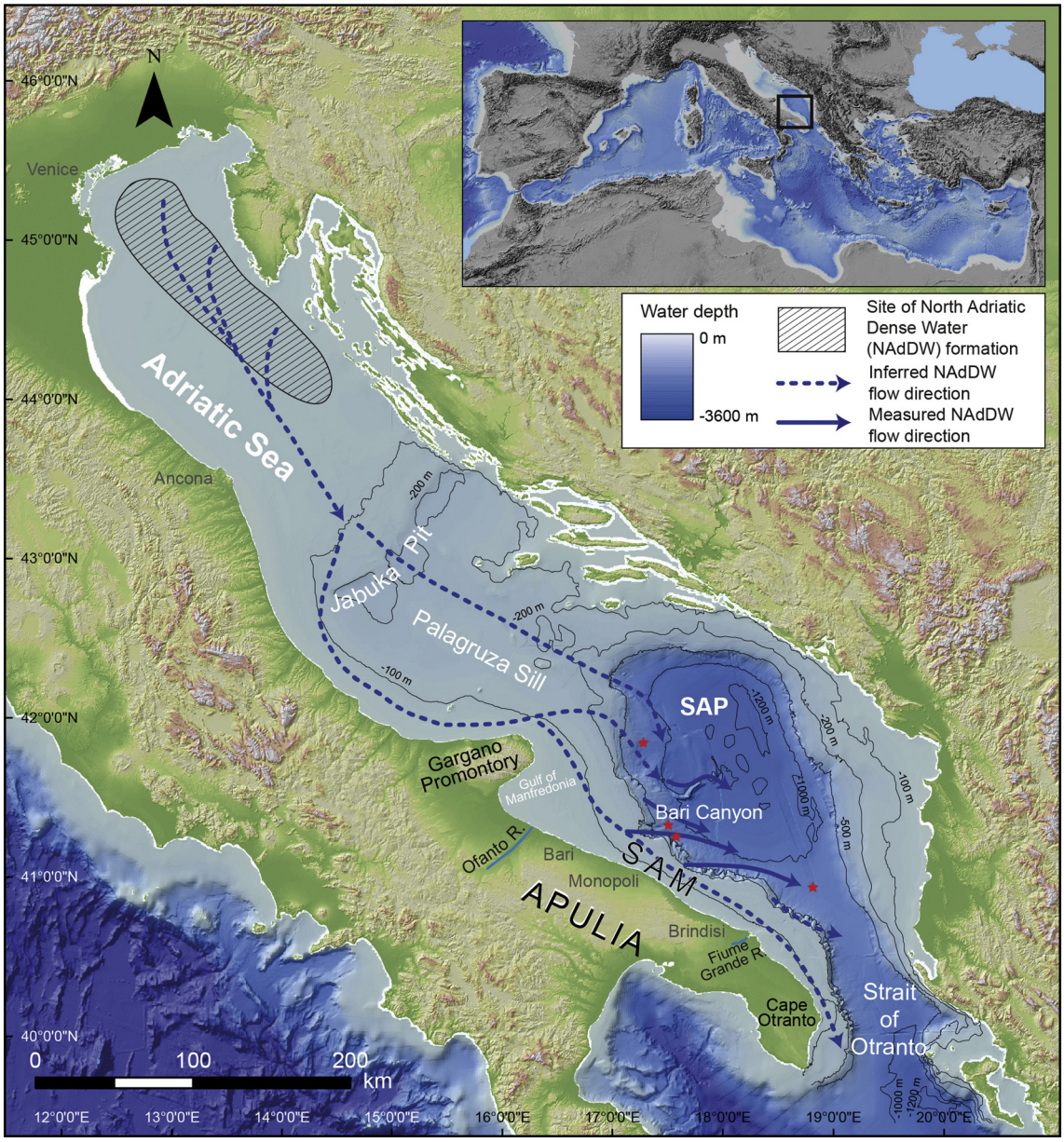

Fig. 1. Bathymetry of the Adriatic Sea area in its Mediterranean context, where the black rectangle delineates the study area (upper right corner). Dotted blue lines and arrows show main inferred paths of the NAdDW, while solid blue lines indicate key sites of its downslope cascading. Red stars show mooring stations (Langone et al., 2016). (For interpretation of the references to colour in this figure legend, the reader is referred to the web version of this article.)

subaqueous progradation (Pellegrini et al., 2015) and increased in strength *ca.* 7.5 kyr BP, as evidenced by the shift of benthic foraminifer oxygen isotope towards higher values (Piva et al., 2008).

3. Geological setting

3.1. Margin morphology

The SAM, south of the Gargano Promontory, has a continental shelf up to 80 km wide in the Gulf of Manfredonia and progressively narrower to the south to a minimum width of 15 km off Cape Otranto (Fig. 1). The shelf edge is rectilinear and erosional north of Bari and becomes more irregular proceeding south, with convex and concave patterns in map view. The most prominent convex sector is about 60 km wide just south of Bari (Fig. 1). The slope average dip increases southward, reaching values between 5° and 10° south of Cape Otranto (Fig. 1). The slope is dissected by gullies and canyons, of which the Bari Canyon is the most prominent feature. Slope-normal canyons and gullies, between 5 and 10 km long breach the shelf edge and may have been active until the last glacial maximum when global sea level was about 125 m below the modern high stand (Siddall et al., 2003). The flow of the contour-parallel NAdDW, testified by the presence of fields of NW-SE furrows, was then responsible for erosion on the upper slope, that led progressively to the disconnection of the canyon heads from the outer shelf (Foglini et al., 2016). The shelf and shelf edge sectors between Brindisi and Otranto (Fig. 1) present along-slope variations of the topographic gradient with relevant erosion where dense waters become accelerated by the local confinement (Pellegrini et al., 2016), while deposition of sediment is favored where the slope is gentler (Bonaldo et al., 2016).

3.2. Sediment sources

The main riverine input comes from the Ofanto River (Gulf of

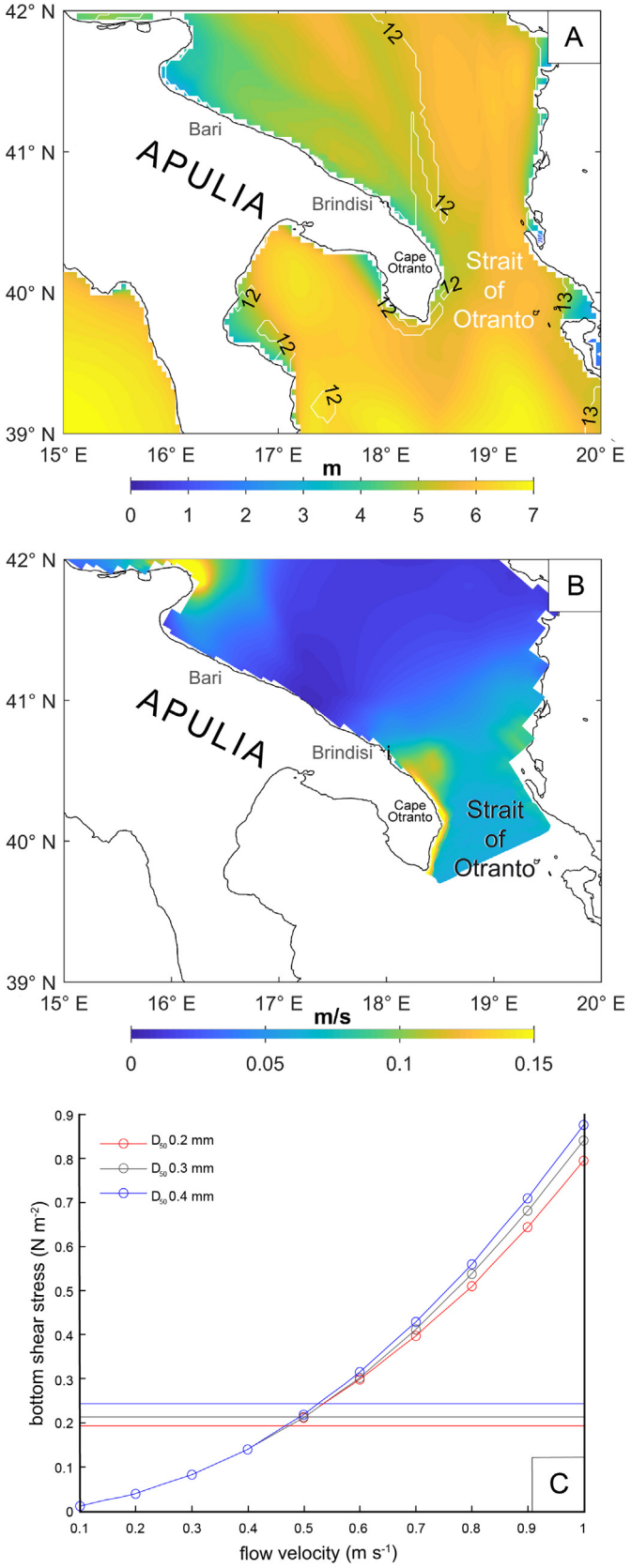

Fig. 2. A. Maximum Hs (colour, [m]) and maximum Tp (white contour, [s]) from CMEMS wave model hindcasts (2010–2016). B. Maximum tidal current from Cushman-Roisin and Naimie (2002) in the Adriatic and from Egbert and Erofeeva (2002) in the Ionian Sea. C. Bottom shear stress plotted against the flow velocity, derived from Kovačević et al. (1999). The colored horizontal lines denote the critical bottom shear stress for 3 grain size classes (D_{50}), which represent average intervals for the SAM bedforms. Dense shelf waters, at least in their most energetic episodes (0.5 m s^{-1}), can generate initiation of motion of the grains.

Manfredonia, Fig. 1), with 1.5 10^6 t yr^{-1}. Except for the Ofanto and the Fiume Grande rivers (Fig. 1), a few intermittent rivers, with seasonal flow regime and torrential nature, are present along the southern coast of the Apulia Region (Cattaneo et al., 2003). Coastal and inner shelf sediment composition reflect highly differentiated drainage basins. Carbonates are abundant and quartz is rare in the southern Apulia Region (south of Cape Otranto), while the Gargano Promontory and the mouth of the Ofanto River are characterized by low percentages of carbonates, mostly represented by dolomite, and abundance of quartz and feldspar. Between the Gulf of Manfredonia and Brindisi, quartz is less abundant compared to the Gargano Promontory, while calcite percentage is generally high (Ambrosano et al., 1986). In the Cape Otranto area, beach sediments do not reflect the carbonate rocks outcropping on land and may come from the Ofanto River through southward transport (Dominici et al., 2016).

3.3. Quaternary stratigraphy

The Quaternary stratigraphic architecture of the Adriatic margin results from the interplay between: high-amplitude (100–120 m) sea level oscillations during the last four 100 kyr glacioeustatic cycles (Trincardi et al., 1994; Trincardi and Correggiari, 2000); progressive seaward tilt of southwestern margin in the last 500 kyr (Ridente and Trincardi, 2002); uneven distribution of riverine sediment input, mostly concentrated north of Gargano Promontory (Cattaneo et al., 2003). The progradation of the lowstand system tract (LST) deposits started about 32 kyr cal BP and ended around 14 kyr cal BP, followed by sediment starvation at the shelf edge (Pellegrini et al., 2017). Last postglacial deposits consist of Late Pleistocene–Holocene transgressive system tract (TST, between 18 and 5.5 kyr cal BP; Pellegrini et al., 2015) and Late Holocene high stand system tract (HST, from 5.5 kyr cal BP to present; Cattaneo et al., 2003), the latter deposited above the maximum flooding surface (mfs).

At the scale of the entire Adriatic basin, muddy HST sediments are confined in < 30–60 m water along the shelf in a pattern that is consistent with the activity of contour-parallel southward flowing bottom-hugging currents, probably represented by the WACC (Amorosi et al., 2016; Cattaneo et al., 2003, 2007; Trincardi et al., 1994). Locally, these HST deposits are organized in small-scale bedforms, the origin of which is still debated between sediment waves (Cattaneo et al., 2004) and limited-displacement sediment failures (Correggiari et al., 2001).

4. Data and Methods

High-resolution bathymetric data of the SAM shelf were acquired between 2009 and 2012, using hull-mounted Kongsberg EM710 (70–100 kHz) and EM3002D (300 kHz) on board R/V Urania and R/V Mariagrazia. Smaller portions of the shelf were mapped at higher detail during cruises undertaken in 2015–2016 on board R/V Minerva Uno, using a pole-mounted Reson Seabat 7125 (400 kHz). Sound velocity profiles were calculated from a Sea-Bird SBE 911 PLUS Current-Temperature-Depth profiler, every 6 h and tide corrections (6–12 cm) were applied in post-processing. All the multibeam data have been merged and post-processed using the software CARIS HIPS & SIPS to produce a 10 m resolution DTM over the entire shelf, and 5 m resolution DTMs over specific bedform fields. Multibeam backscatter data, acquired with the Reson Seabat 7125 multibeam system, were processed with the software QPS Fledermaus FMGT module.

Sub-bottom seismic profiles were acquired with a Teledyne Benthos

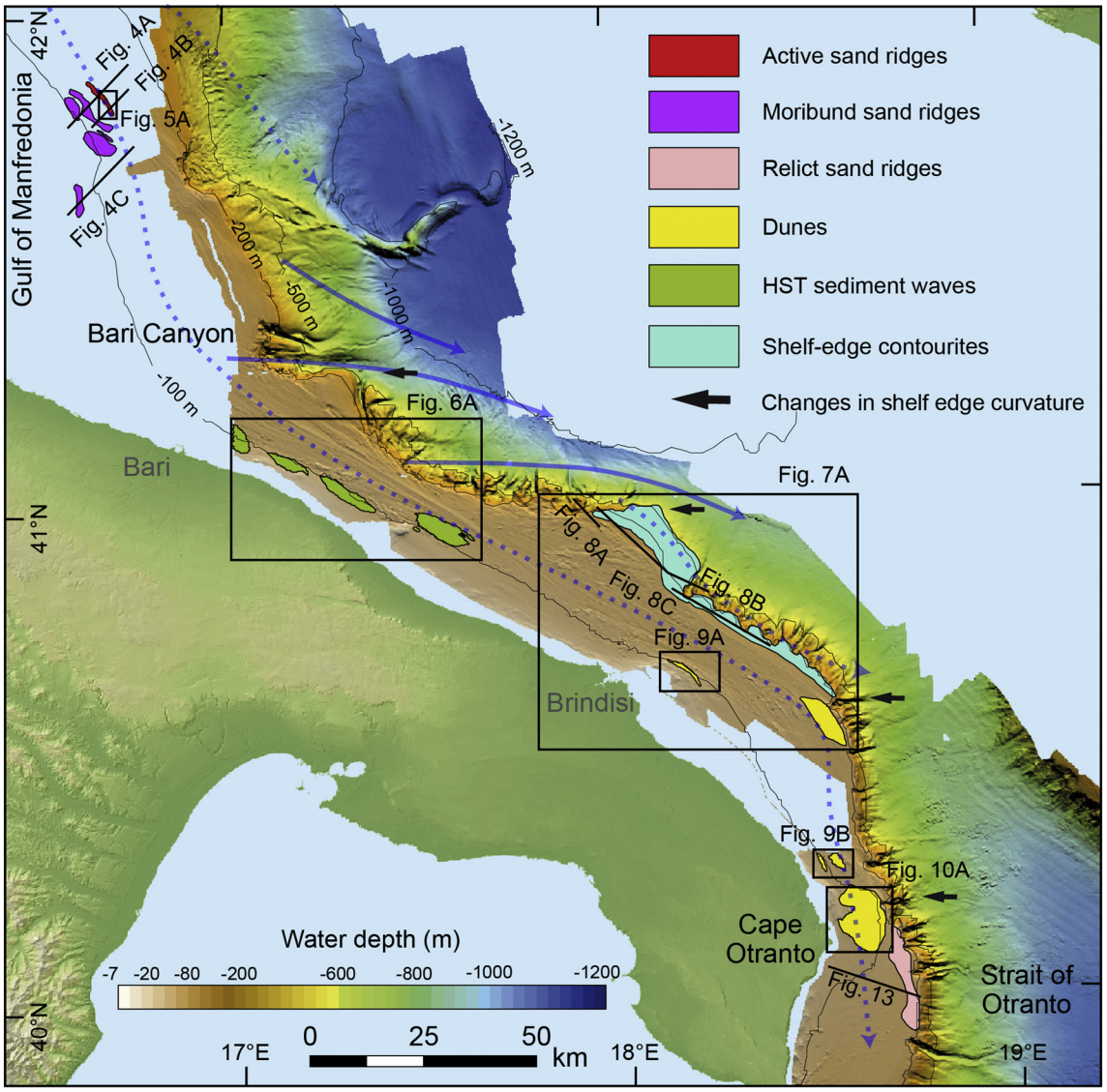

Fig. 3. DTM of the bathymetry derived from the compilation of different multibeam surveys in the SAM (20 m grid, vertical exaggeration 10×). The map shows the location of the bedform fields (colour coded) and the location of the figures which illustrate them. Blue dotted arrowed lines indicate the path of the NAdDW inferred from the morphology and internal structures of the bedforms of this study, blue solid lines refer to Fig. 1. (For interpretation of the references to colour in this figure legend, the reader is referred to the web version of this article.)

CHIRP-III system, composed of a 16 hull-mounted transducer array, using a 2–20 kHz sweep-modulated bandwidth and 4 kW power per-channel, which allows a vertical resolution of about 50 cm, on board R/V Urania and Minerva Uno.

Sparker profiles were acquired with a Geo-Spark 1000 (1 kJ) source and recorded with a towed Edgetech 265 hydrophone, in 2015 and 2016 on board R/V Minerva Uno. Seismic profiles were post-processed using the GeoSuite AllWorks software, applying a standard sequence including zero-phase 300–2000 Hz band pass filter, automatic and time-variant gain and median filters.

Sub-seafloor sediment samples were collected using a Geo-Corer 6000 vibrocorer, provided by GEO Marine Survey Systems b.v., using a 6 m long barrel. Surficial samples were collected either with a Van Veen grab or a light (100–300 kg) corer with a 104 mm diameter, designed to recover the undisturbed bottom-seawater interface and used for sedimentation rates estimates.

Grain size analysis was performed by sieving and for the < 63 μ fraction a Micrometrics SEDIGRAPH III 5120 was used. A uniform set of statistical parameters was calculated using the GRADISTAT grain size distribution and statistics package. Bulk mineralogy of the sediment was analyzed by X-ray diffraction on powdered samples, using a Philips PW 1130 diffractometer, applying 40 kV accelerating voltage and 30 mA current (detection limit 0.1%).

AMS ^{14}C radiocarbon dating was performed on a number of bivalve shells at Beta Analytic Inc. Laboratories in Miami (U.S.). The results were adjusted for the local reservoir correction (ΔR = 121 ± 60 yr). Calibration was performed with BetaCal3.21, High Probability Density Range Method: MARINE13.

Samples were frozen to −20 °C, freeze-dried and then analyzed for ^{210}Pb and Sediment Accumulation Rate (SAR) estimates. Sediment porosity was determined from the water content, assuming a mineral density of 2.5 g cm^{-3}. Alpha counting of ^{210}Po was used for ^{210}Pb determinations, assuming secular equilibrium between the two isotopes, for a detailed description of the methodology see Frignani and Langone (1991).

The shape characteristics of the bedforms were calculated from the simple equations of Knaapen (2005), where the wavelength is the distance between the trough positions on opposite sides of a crest. The height is defined as the difference between the crest and the baseline of two adjacent troughs; the asymmetry (A) is characterized as the

difference of the distance between crest and troughs located on the opposite sides and divided by the wavelength. The effect of the regional seafloor slope on these calculations is negligible in the study area, because it is < 1°. Bedform parameters were calculated along bathymetric transects generally oriented orthogonal to the main crest alignment and according to the bedforms' main orientation. Indeed, the direction of asymmetry of bedforms is used to map bedload transport paths (Van Landeghem et al., 2009). Thus, indicatively, A < 0 shows northward-directed transport, A > 0 indicates southward-directed transport, A = 0 indicates the presence of symmetric bedforms with no inferred net transport directions. This criterion is used to describe the general trend of the shelf, although sediment waves geometry has been found poorly indicative of their sense of migration in modern tidal settings (Van Landeghem et al., 2012), where sediment waves migrate also in the direction of their gentle stoss slope.

The bearing direction of the downhill slope of each field of bedforms was calculated using the ESRI ArcGIS 10.5.1 tool "aspect", on a projected flat plane using a 2D Cartesian coordinate system. In this case, we used a filtered 25 m resolution DTM for the entire shelf area. Aspect is expressed in positive degrees from 0 to 360, measured clockwise from north.

5. Results

The entire sedimentary succession of the western Adriatic margin has been age-constrained based on the calibration of seismic stratigraphy with a set of multi-proxy chronological data derived from sediment cores and borehole data (*e.g.,* Pellegrini et al., 2018). From these regional correlations, we derive the stratigraphic interpretation of the seismic profiles.

In particular, last postglacial deposits are bounded by Erosional Surface 1 (ES1), while Erosional Surface 2 (ES2) records sea level rise from Isotope Stage 6 to Stage 5 (Trincardi and Correggiari, 2000). For its largest part, the SAM shelf is sediment starved, with the dominance of erosive remnants of diverse size (relief and extent) but consistent shore-parallel orientation, which are made up by deposits that rest above the ES1 and ES2 surfaces.

5.1. Sand Ridges off Gulf of Manfredonia

The shelf in the Gulf of Manfredonia is characterized by the presence on the seabed of sandy lenticular deposits (Fig. 3). These deposits show a variable width between 500 and 1500 m and reach thicknesses of up to 9 m (Fig. 4 and Table 1). Overall, these deposits occur in water depths between 90 and 115 m and are elongated roughly parallel to the bathymetric contours in a NW–SE direction.

The sand ridge located closer to the shelf edge (115 m water depth) is 10 km long, 1 km wide, 7–9 m in thickness and is exposed at the seafloor (Fig. 3). This sand ridge attains a maximum seaward slope of 5° in its northern sector (Fig. 4A), where it is characterized by internal high-amplitude, continuous, oblique reflections with up to 6° dip (Fig. 4A); whereas in its southern sector the sand ridge shows high-amplitude, continuous, gentler sigmoid-oblique reflections with < 2° dip (Fig. 4B). A drape of muddy deposits up to 5-m-thick buries other similar sand ridges located more landward (Figs. 3, 4C).

The sand ridge located at 115 m water depth displays superimposed bedforms with a maximum height and wavelength of 2 m and of 200 m, respectively, and with a steep lee side facing south (Fig. 5A, B). Grain sizes (D_{50}, Table 1) of the seabed sediments trend to increase from north to south, along the sand ridge (Fig. 5C).

5.2. Small-scale muddy bedforms

Small-scale bedforms are present south of Bari (Fig. 3, Table 1), in the bathymetric range of 70–100 m stretching for almost 70 km along the shelf (Fig. 6A, E) and are organized in four main fields, with the southern one (field 4) developing in slightly deeper waters (100–115 m). Field 1 (Fig. 6A) shows maximum heights of 2 m and average wavelengths 50–100 m, bedforms crests are WNW–ESE oriented, roughly parallel to the bathymetric contour (Fig. 6B). Bedforms in field 2 can reach up to 3 m in height with wavelengths of 100–200 m and crests oriented NNE–SSW with a progressive reorientation of their steepest lee sides from facing N–NE to S–SE proceeding southward along the field. Field 3 has bedforms with heights of 2 m and maximum wavelengths of 200 m, with crests NW–SE oriented; their steepest lee sides face E-SE. Landward, the fields connect to other bedforms (seafloor undulations *sensu* Cattaneo et al., 2004), which are best identified by the seafloor backscatter (Fig. 6C, E), where their rounded crests exhibit a preferred alignment in the opposite NE–SW direction. The lateral continuity and linearity of the crests of these bedforms, which develop where the mud wedge is confined in the inner shelf and < 10-m-thick, decreases with increasing water depth, where they become more sinuous.

The first three fields are topographically delimited seaward by linear erosional remnants draped by a thin (< 1 m in the CHIRP profiles) seismically transparent layer or exposed at the seafloor in water depths > 120 m (Fig. 6A). Giant scours up to 10 m deep, 1 km wide and 5 to 20 km long, are present in water depths > 120 m and appear parallel to the shelf edge. The deeper-water bedforms (field 4) are characterized by heights of 0.5 m, wavelengths similar to the other fields, crests oriented NNE–SSW and lee sides facing eastward (Fig. 6A).

The CHIRP profiles (Fig. 6F) indicate that the muddy bedforms develop above the mfs, while the underlying TST is characterized by uniform and continuous plain-parallel reflection packages. This evidence suggests a significant increase in bottom current regime, which affects the sedimentation pattern during the HST.

5.3. Erosional features and longitudinal bedforms

The shelf sector offshore Brindisi (Fig. 3) is characterized by marked seafloor roughness. Small-scale bedforms alternate with large contour-parallel flute-shaped scours up to 20 m deep, located close to the shelf edge, and furrows, highlighting large variability in seafloor erosion (Fig. 7A). Comet marks normally form under peak velocities impacting an obstacle, developing a tail of erosion in the rear. A giant (23 km long) and complex comet mark-like feature is present where the shelf is 36 km wide. In this case the obstacle is a 7 km long outcropping substrate, roughly oriented WNW–ESE, cemented atop by calcareous algae. Under the action of bottom currents, the erosive tails tend to form elongated sand ribbons at their sides (Fig. 7A). The longitudinal sand ribbons seem to indicate an almost SE-oriented flow direction towards the shelf edge. Comet marks are present especially where the obstacles are represented by 5–10 m high reliefs and the erosive tails can be up to 3 km long (Fig. 7B), showing a consistent orientation with the corresponding sand shadows (*sensu* Flemming, 1980) upcurrent (Fig. 7A). In the study area, erosive tails tend to have modest length (few hundred meters), especially if compared to the sand shadows forming at their sides, which have km-scale lengths. The length/width ratio of the erosive tails is relatively small (in the order of 5 times), which indicates the action of moderate bottom unidirectional flows with maximum near-bottom velocities of 0.6 m s^{-1} (*e.g.,* Kuijpers et al., 2002).

Farther offshore, seafloor sediments are made of reworked glacial and postglacial deposits (Fig. 7C), distributed in a complex pattern of sediment types with a variable biogenic component.

5.4. Sediment drifts at the shelf edge and upper slope

Off Brindisi, the continental shelf is larger (*ca.* 40 km, Figs. 3 and 7A) and the Late Quaternary deposits are mostly exposed at the seafloor. These Late Quaternary deposits are characterized by erosional features and remnant ridges oriented *ca.* NW–SE (Figs. 7A and 8). On the outer shelf and upper slope, sediment deposits up to 50-m-thick are

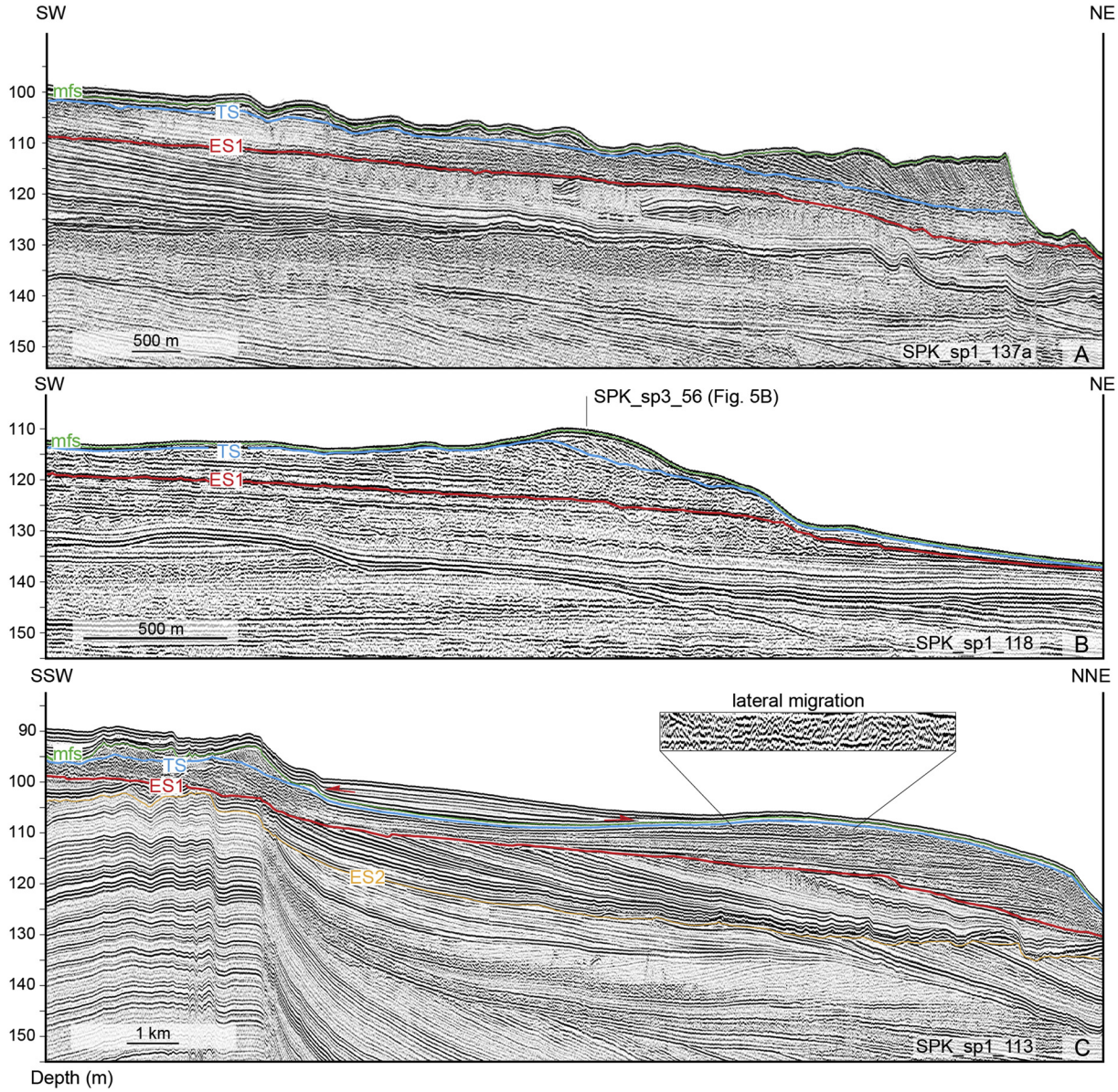

Fig. 4. A. Sparker seismic profile across the northern sector of the active sand ridge. B. Sparker seismic profile across the southern sector of the active sand ridge. The stratigraphic unit between ES1 and TS is characterized by high amplitude, continuous and parallel reflections that pass laterally to high amplitude and chaotic reflections with locally high-angle dipping reflections. C. Sparker seismic profile across the moribund sand ridge. Above the mfs, high amplitude and continuous reflections with local bidirectional downlap terminations characterize the muddy HST. Location of the seismic profiles and of the sand ridges is given in Fig. 3.

characterized by mounded-parallel and continuous reflections (Fig. 8). Sediment drifts and erosional moats form where the shelf edge makes a seaward bulge (Fig. 3) and the upper slope is dissected by short (5–10 km in length, 1 km in width) and straight canyons (Fig. 7A). Both drifts and moats elongate parallel to the shelf edge and can be ascribed to contourite deposits like those increasingly recognised in shallow-water settings, where the influence of geostrophic currents prevails over storm and wind-induced currents above 300 m water depth (Viana et al., 2007; Verdicchio and Trincardi, 2008). On the slope-facing flank of the drift, the deposits pass to semi-transparent seismic facies with low-amplitude and discontinues reflections, reminiscent of mass-transport deposits (Fig. 8A, B). On their up-dip flank, the contourites show upward-convex reflections with truncated terminations, suggesting areas of local enhanced erosion between 150 and 350 m water depths (Fig. 8A, C). In the shaded relief of the bathymetry, these areas of local erosion correspond to moats, canyon heads and deep scours (Fig. 7A).

5.5. Topography-constrained large dunes

Along the shelf, there are several examples of sand dunes which develop landward of topographic ridges, such as erosive remnants cemented by variable components of coralligenous bioconstructions (Table 1). Large sand dunes located just 15 km off Brindisi (Fig. 3) in 90 m water depth, develop on a sub-horizontal seafloor and landward of a 5 m high, bowed ridge stabilized by encrusting calcareous algae and invertebrate associations (vibrocoring station SP1_03) and seaward of a wave-cut terrace, that together act as an obstacle likely accelerating bottom currents (Fig. 9A). Dunes are linear and 1 m high in the north, with crests oriented N-S, and change southward into barchan-like 2 m high dunes, spaced between 100 and a maximum of 300 m. Dunes ramp slightly up dip from 94 to 85 m southward and show a slight asymmetry with the lee sides facing the SE (N112–157°E). Wavelengths increase southward from 100 to 300 m (Fig. 9A).

Another field of large dunes is located 7 km off the coast, north of

Table 1
Detailed description of all depositional sedimentary bodies along the SAM shelf, in respect to their location and shelf morphology, including their paleoenvironmental interpretation.

Location	Max height (m)	Wavelenght	Orientation	Water depth (m)	Grain Size (D_{50}, mm)	Seismic Facies	Stratigraphic position	Paleoenvironment interpretation
Around promontory, shelf edge (Gulf of Manfredonia)	9	500–1500	NW–SE	90–115	0.2–0.4	High-amplitude, continuous, oblique and complex sigmoid-oblique reflections	above TS	Transgressive shoreface sand ridges, active and moribund
Topography constrained, narrow rectilinear mid/inner shelf	4	50–100	WNW–ESE	70–115	Mud	High-angle dipping reflections and hyperbolae	Above mfs	Mid shelf sediment waves
Curved outer shelf/upper slope	50	1000	NW–SE	120–300	mud	Mounded-parallel and continuous reflections	Above es1	Shelf edge contourites
Topography constrained, outer shelf	2	100–300	NW–SE	9–100	0.2–0.3	High-angle dipping reflections	Above ts	Mid shelf dunes
Sediment-starved, curved outer shelf	3	200–400	WNW–ESE, ENE-WSW	115	0.12–0.15	High-angle dipping reflections and hyperbolae	Above ts	Mid shelf dunes
Around promontory, narrow outer shelf (Cape Otranto)	6	200–500	NW–SE, ENE–WSW	80–100	0.2–0.4	High-amplitude and high-angle dipping reflection, above stacked clinoform deposits	Above ts	Shoreface-connected ridges
Narrow curved shelf edge (Strait of Otranto)	5	700	N-S	120–130	0.5–1.5	High-amplitude, continuous, sigmoid to oblique reflections	Above es1	Lowstand shoreface ridges, relict

Cape Otranto, in 100 m water depth (Fig. 3), 2D crests are oriented N20°E oblique to the coast (Fig. 9B). The dunes are up to 2 m high, have 200 m wavelengths and show slight asymmetry to the SE (N112–157°E). They are located landward of a 6 m high terraced erosive remnant (Fig. 9B). The CHIRP seismic profile perpendicular to the crest orientations (Fig. 9C) shows, in the seismic unit between ES1 and ES2, buried climbing dunes in the NW with concave foresets and depositional stoss slopes. The apparent direction of motion of the buried bedforms is towards the NW, opposite to the present-day dune field at the seafloor. Locally, buried bedforms have an angle of climb exceeding their stoss slope angle, which seems to increase upward (Fig. 9C). Paleo-flow direction is less straightforward to infer in this case. All buried bedforms appear to be eroded at their top by the ES1 surface and are indicative of a different oceanographic regime before the last lowstand (Fig. 9C).

Other dunes that appear to be influenced by the local morphology of the margin, in sediment-starved conditions, are presented in Fig. 7B, they are up to 3 m high and show wavelengths of several hundred meters (Fig. 7D). Crest orientations slightly change following the convex shape of the shelf edge from WNW–ESE to ENE–WSW, with lee sides facing S and SE (Fig. 7B).

5.6. Large and very large dunes off Cape Otranto

A broad (57 km^2) heterogeneous field of large to very large dunes occurs at 80–93 m water depth, down current of an up to 15 m high NE-SW oriented outcropping rocky ridge offshore Cape Otranto (Fig. 10A). The dunes show variable wavelengths and are rectilinear to sinuous in shape, displaying variable crest orientations, roughly from ENE–WSW in the northern part to NW–SE in the southernmost portion of the field (Table 1).

Landward, 2D straight dunes with rounded crests (Fig. 10B) striking in the E–W direction cover an area of 9.3 km^2. They are 1 to 4 m high and have wavelengths of 200–350 m, mostly symmetric or slightly asymmetric (max 0.5) towards the S–SE (N157–202°E, N112–157°E). On the eastern edge of this sector, there is a parting zone where bedforms are 3 to 4 m high and characterized by a slight asymmetry (max –0.28) with their lee sides facing the opposite N–NE direction (up to N67°E) (Fig. 10A).

Farther offshore, the field bifurcates into: a northern sector where bedforms maintain a linear shape with attenuated rounded crests striking in the E–W direction changing to ENE–WSW; and a southern sector of 3D bedforms with shapes from sinuous to barchan-like and occasionally trochoidal, with a sharp change in the orientation of the crests in a preferred NW–SE crest direction (Fig. 10A). The northern sector is characterized by 1 to 2 m high symmetric dunes with wavelengths of 400 m (Fig. 10C), the heights increase up to 4 m at the eastern limit of the bedform field. Bedform heights and wavelengths progressively increase to respectively 6 m and 500 m with asymmetry (average 0.6) to the south (Fig. 10C). The southern sector presents a more irregular pattern of large-scale asymmetric and sinuous bedforms with superimposed smaller and linear dunes 200 m wide and 2 m high, with lee sides consistently facing S (N157–202°E). Both larger and smaller-scale bedforms share the same alignment along the NW–SE direction (Fig. 10A).

Closer to the shelf edge, isolated and less developed dunes are detached from the main bedform field by an area of flat seafloor. The isolated dunes are 3 to 6 m high, have variable wavelengths, moderate asymmetry with southerly facing lee sides (Fig. 10A), and display trochoidal to slightly sinuous or linguoid shapes, suggesting sediment-starved conditions leading to poorly formed 3D dunes.

Sparker profiles, across the whole dune field (Fig. 10D), document the variable asymmetric shape of the dunes, with overall increasing southward facing asymmetry proceeding south. The dunes develop well above ES1, having the TS as their lower bounding surface (Fig. 10C, D). Below ES1, variable dip reflection packages (green dotted lines in

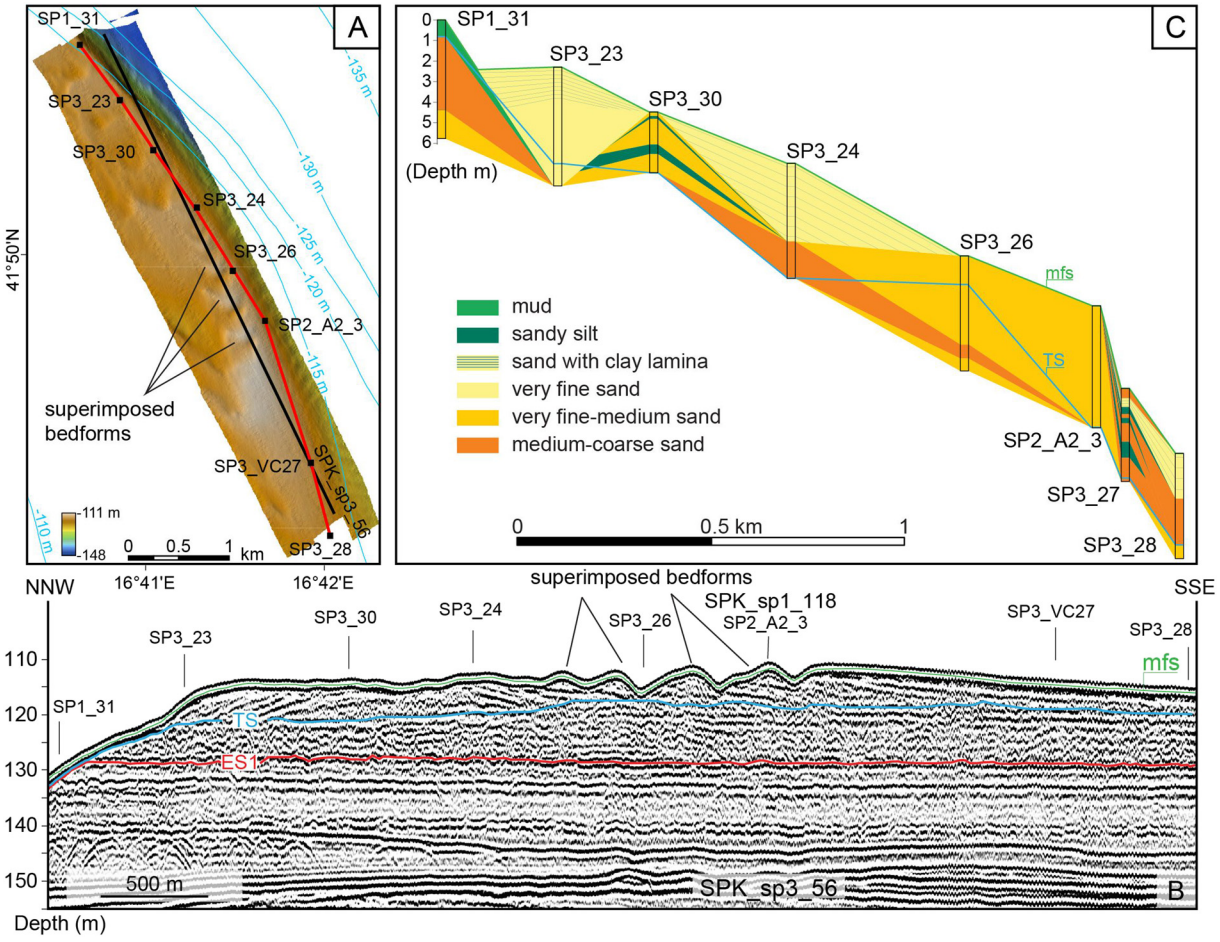

Fig. 5. A. 5 m resolution multibeam DTM acquired over the southern sector of the active sand ridge, with location of the seismic sparker profile displayed in B (Fig. 3 for location). Colour palette is the same for all figures, but the scale changes according to the bathymetric interval. B. Sparker seismic profile over the crest of the active ridge showing the superimposed bedforms. C. Fence diagram based on the vibrocoring samples acquired along the ridge (location in A). The presence of sandy silt layers along the sediment cores (cores SP3_30 and SP3_27) indicates distinctive relatively lower-energy depositional phases.

Fig. 10D) seem older stacked dune deposits of variable thickness. The TS surface becomes exposed in the troughs, and at places amalgamates with ES1 (Fig. 10A, D) and correlates well with an enhanced seafloor backscatter (Fig. 10E). The straight dune crests appear as shades of low backscatter, which correspond to mixed quartz and carbonate fine to medium sand. Darker shades (high backscatter) in the through denote coarse shell and limestone gravel; occasionally this coarser lag is overlain by up to 2 m of fine sand with clay lamina, as in core SP2_19 (lighter gray, Fig. 10D, E). Marine mollusk shells retrieved from the lower bounding surface, indicative of water depths 20–50 m, have been radiocarbon dated and show ages not older than 13,319–12,961 cal BP (TS in Fig. 11B, Table 2). In the eastern sector of the dunes field, above the TS, high amplitude and high-angle south-dipping reflectors correspond in sediment cores to highly bioturbated layers, with occasional laminations or shell lags. Shells are mostly of marine species *Atrina fragilis*, *Capulus* sp. and *Pecten* sp. and have been radiocarbon dated in several cores between 9885 and 11,180 cal BP (Fig. 11 and Table 2). In terms of grain size, finer sands (D_{50} = 0.21 mm) are more often found in the southern sector of the field (Table 1). Mineralogic composition is quartz, with carbonates representing a mere 20–30% (Fig. 12A), which significantly differs from the onshore counterpart. Seafloor benthic assemblages include *Acanthocardia aculeata*, *A. fragilis*, *Capulus.* sp. Two specimens of *A. fragilis* retrieved 15–20 cm below the seafloor were dated 650–450 cal BP and 734–514 cal BP, while one specimen of *Capulus.* sp., collected at the seafloor, was dated Post 1950 CE (Fig. 11 and Table 2). Short-lived ^{210}Pb radionuclides in shallow samples document lateral variations in sediment accumulation rates (SAR) between crests, with rates as low as 0.4 mm yr^{-1}, and troughs with 0.9 mm yr^{-1} (Fig. 12B). The SAR is six fold higher (up to 2.3 mm yr^{-1}) outside the bedforms field (SP3_gr01, Figs. 10, 12B), indicating a less dynamic environment there.

5.7. Sand Ridges in the Strait of Otranto

The shelf sector in the Strait of Otranto stretches up to 26 km and, at depths > 120 m, linear sand bodies up to 5 m high and 700 m wide are present close to the shelf edge (Table 1). The sand bodies have symmetric rounded crests and are elongated in N-S direction, parallel to the coast. This sector is today sediment-starved as documented by the occurrence of the ES1 surface almost at the seafloor (Fig. 13). The sand body located at the shelf edge is characterized by high-amplitude, continuous, sigmoid-oblique reflections, while the sand bodies located in a more proximal position are characterized by high-amplitude, continuous, oblique and dipping reflections (up to 6°; Fig. 13). The dipping reflections show downlap terminations above ES1. High-amplitude and continuous reflections overlie the foresets (Fig. 13). Sediment cores on the ridge crests collected 1 m of mud sealing 4 m of coarse and very coarse sand, while in the troughs the mud drape is limited to a few decimeters.

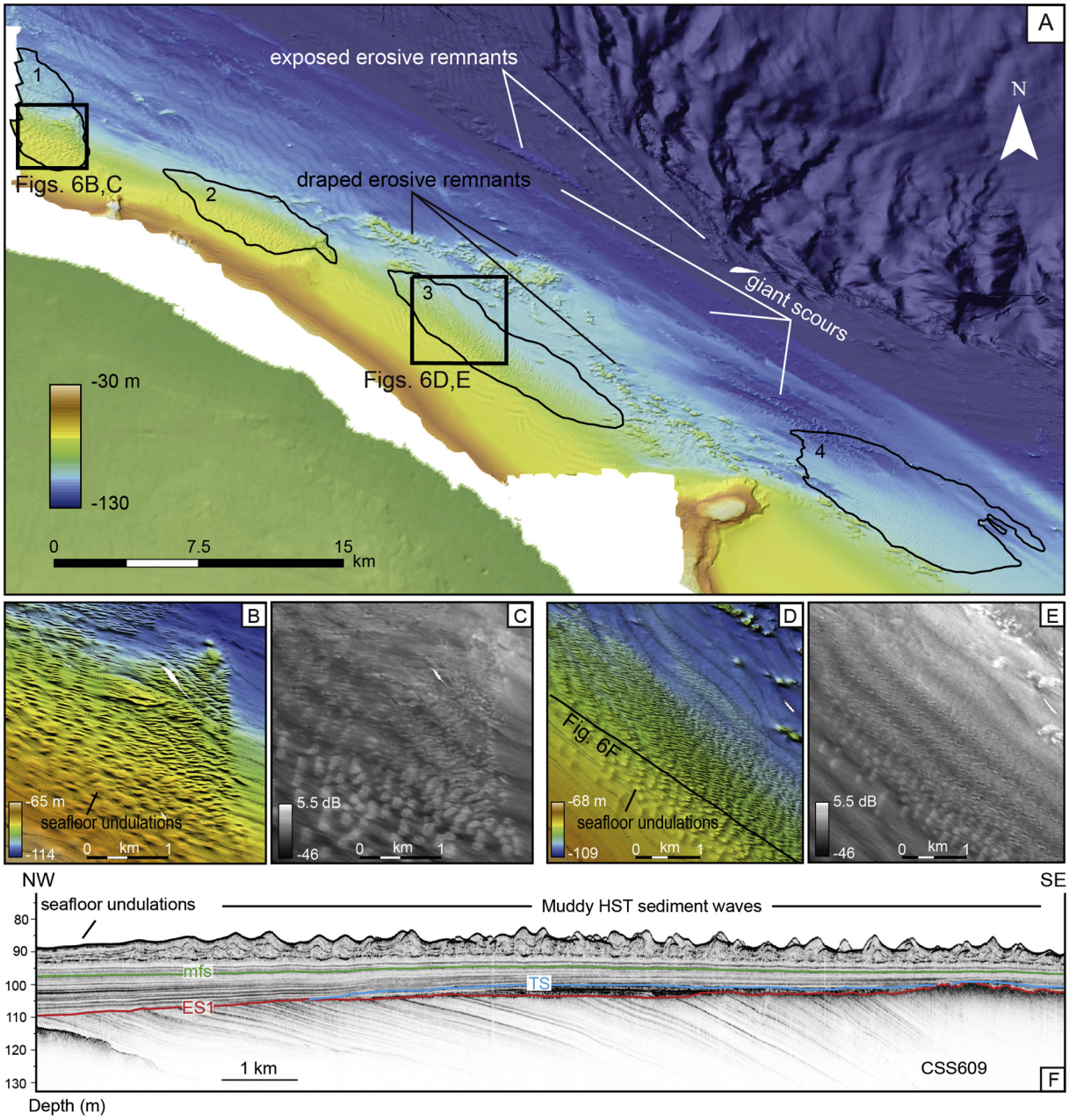

Fig. 6. A. Bathymetry (10 m resolution) of the shelf sector (location in Fig. 3), where four principal fields of small-scall bedforms are observed (black polygons). B and D: 5 m resolution DTMs (vertical exaggeration 10 x) of insets of bedforms fields 1 and 3. C and E: seafloor backscatter of B and D areas. F. CHIRP seismic profile across one of the small-scale bedforms fields showing the seafloor undulations and the muddy sediment waves developing on top of the maximum flooding surface (mfs). Internally high-angle dipping reflections suggest the coalescence of smaller individual buried bedforms. Location of the profile in D.

6. Discussion

6.1. Paleoenvironments of the large-scale sandy bedforms

Sand ridges located off the Gulf of Manfredonia developed above the TS, topping reworked lowstand deposits. The surface at their top coincides with the mfs. Therefore, these ridges formed between the lowstand and the early stage of sea level rise as documented on several wave-dominated continental margins in the Mediterranean area (Bassetti et al., 2006; Berné et al., 1998). In the Gulf of Manfredonia, pronounced seafloor morphology and high-angle clinoform progradations occur only in the sand ridge located at the shelf edge (Fig. 4A), while the other ridges in shallower depths have lower-angle internal reflectors and are draped by HST muddy sediment (Fig. 4C). Normally, well organized dipping strata with a progressive seaward increase in foreset angle indicate appreciable progradation and may occur anytime during the postglacial sea level rise (Park et al., 2003; Snedden et al., 2011).

Thick sandy lowstand shorefaces from wave-dominated settings are elongated roughly parallel to the coast (Berné et al., 2002) and this can be considered an empirical criterion to distinguish them from obliquely or shore-normal transgressive sand ridges. Sand ridges in the Strait of Otranto, which still cause seafloor relief although buried below HST m-thick muddy sediment, extend parallel to the coast at 118–130 m water depth and show aggradation at their topsets. Their lower bounding surface regionally correlates to ES1, formed at the peak of the last glacial lowstand, and thus can be ascribed to lowstand shorefaces (Table 1).

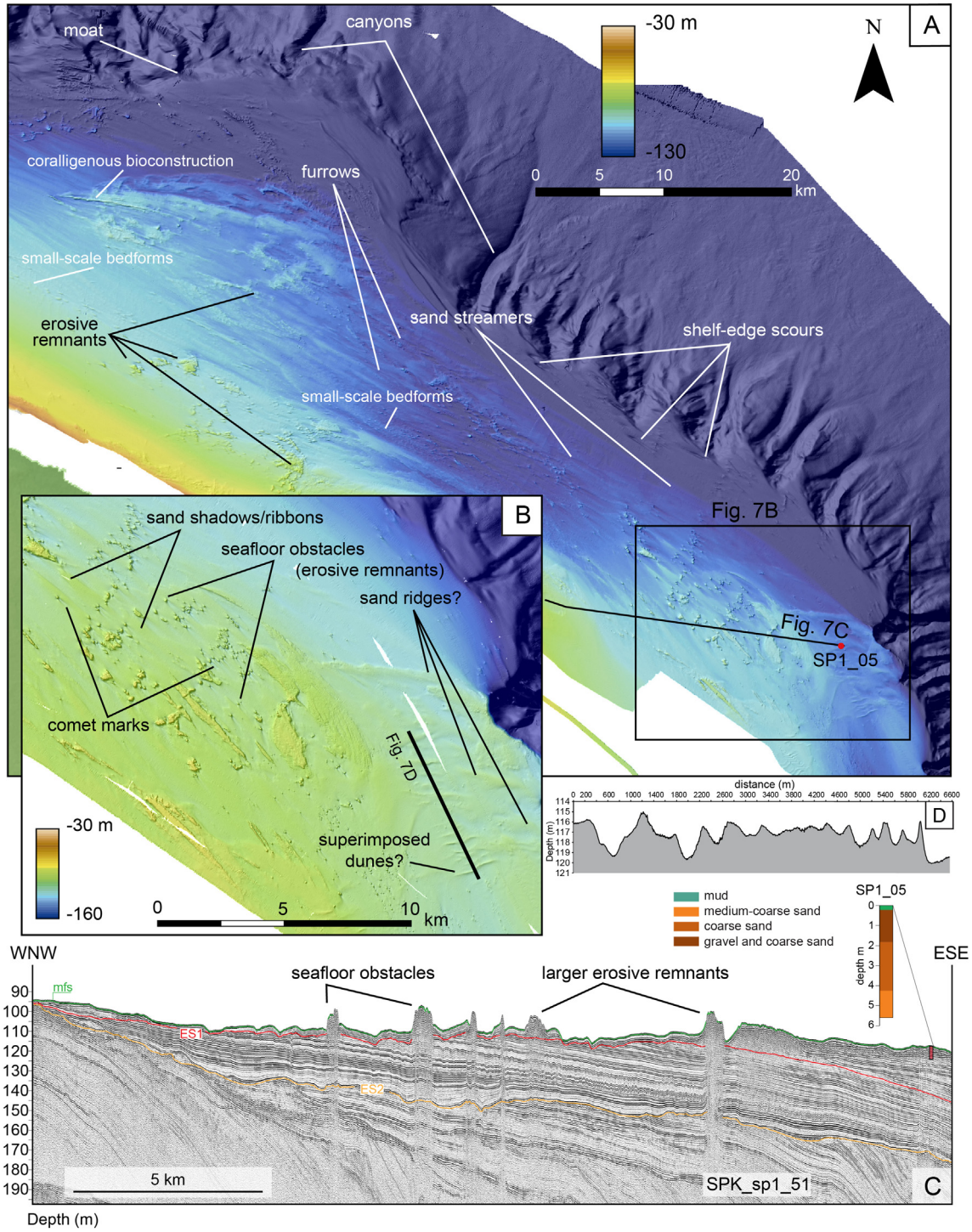

Fig. 7. A. Bathymetry of the sediment-starved shelf sector (25 m resolution), location in Fig. 3. B. 10 m resolution DTM of the inset highlighted by the black rectangle in A. C. Sparker profile across the shelf sector with location and log of coring sample SP1_05. D. Bathymetric profile across the dune field of B.

The morphology, internal structure and orientation of some of the Otranto dunes are comparable to sand ridges described on storm-dominated continental shelves. Storm-dominated ridges normally show internal high-angle reflectors dipping in the direction of the steepest side (*e.g.,* Li and King, 2007). The eastern Otranto dunes in fact show linear, elongated shapes with orientations oblique to the shoreline, and display internal high-angle reflectors dipping in the direction of the steepest side (Fig. 10C) or lower dipping angles when the degree of asymmetry of the dunes is lower (Fig. 10B). In the southern sector of the dunes field, juvenile storm-built shelf sand ridges may develop from a pre-existing bathymetric feature (precursor), which provides a nucleation point (Snedden et al., 2011). The presence of pits and depressions on the ravinement surface (Fig. 10D), which acts as the lower bounding surface of the bedforms, is indicative of a precursor topography typical of the shoreface-connected ridges (Edwards et al., 2003; Swift et al., 1978). Furthermore, inner shelf ridges, oblique to the coast, have been observed also in relatively low energy shore-parallel flow (0.2 m s^{-1}) and sediment-starved settings (Edwards et al., 2003), suggesting that they do not require high energy from severe storms to form. High-amplitude dipping reflectors within the Otranto dunes correspond to

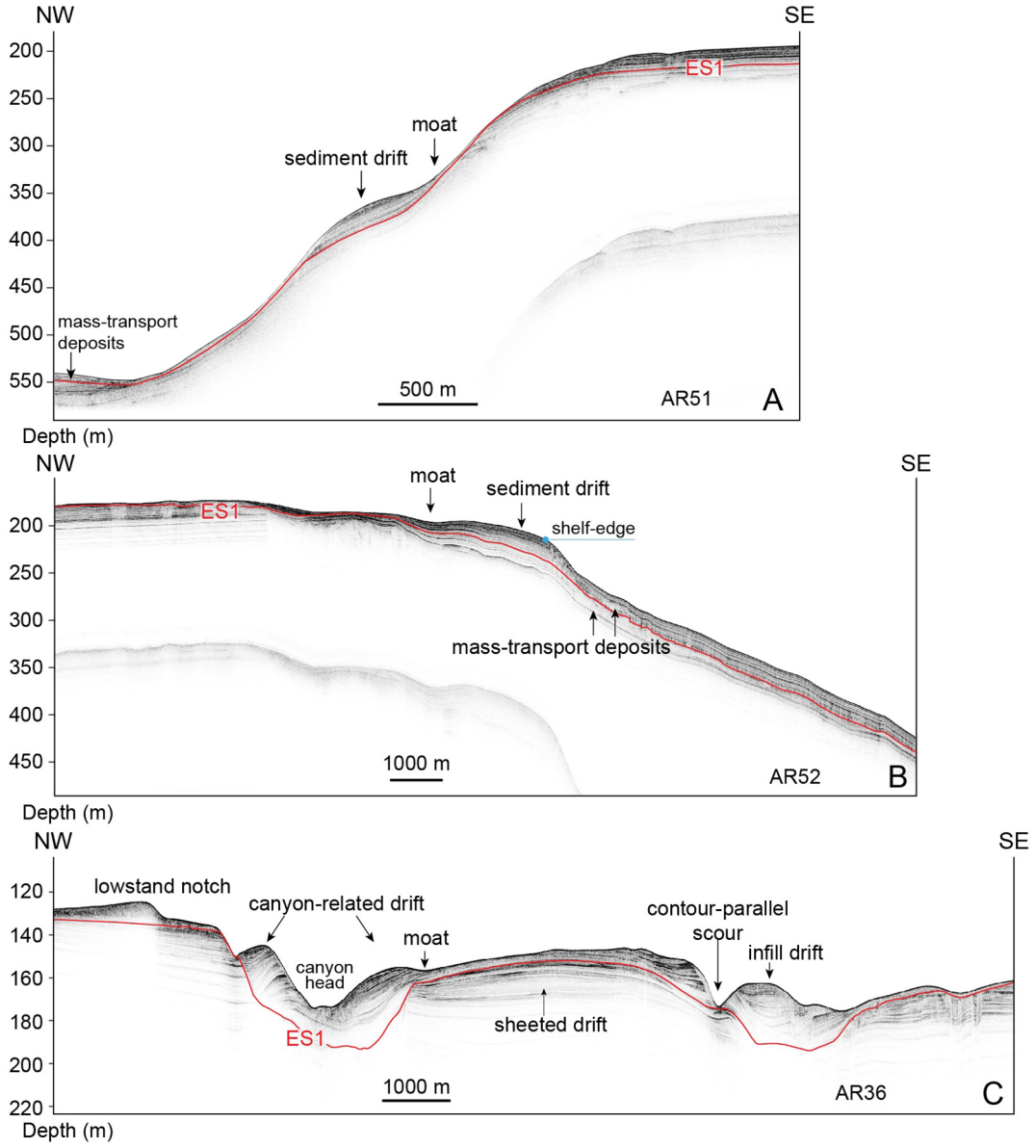

Fig. 8. A. CHIRP seismic profile across the upper slope showing an erosional moat and a corresponding sediment drift. B. CHIRP seismic profile along the shelf edge and the upper slope, showing an erosional moat and a sediment drift on the shelf. C. CHIRP seismic profile along the upper slope showing the complex pattern of erosion and deposition. Location of the seismic profiles in Fig. 3.

silty and sandy mud beds, lag of shells and bioturbation in the sediment cores, which might represent a drape of internal dipping surfaces, suggesting that sand ridge migration is likely episodic.

6.2. *Timing of formation of the large sandy bedforms*

Numerous studies have suggested that sand ridges and large-scale bedforms, now lying on the outer shelves of the Mediterranean Sea, formed during the last post-glacial sea level rise and record in particular intervals of decelerated rise or stillstand. As an example, in the Gulf of Lyons and on the Murcia shelf, coastal sands formed around the Younger Dryas cold reversal (11.5 to 12.7 kyr BP), in water depths 50–60 m below the present sea level (Bassetti et al., 2006; Durán et al., 2017). This interpretation derives from a simple rule-of-thumb equation: H = 0.167 h (*cf.* Yalin, 1992), where H is the maximum bedform height and h is the original water depth where it formed. Hence, sand ridges formed in a shallower marine environment than today and became preserved by subsequent accelerated sea level rise (meltwater pulse 1B, Fig. 14), which favored their preservation, avoiding their dismantling by coastal hydrodynamic processes.

Applying these calculations to our case studies, it derives that sand ridges off the Gulf of Manfredonia developed starting around the Younger Dryas, while sand ridges in the Strait of Otranto may have formed earlier, just before meltwater pulse 1A (Fig. 14). The Otranto dunes started forming slightly earlier than the sand ridges located off the Gulf of Manfredonia (Fig. 14), which is in agreement with the radiocarbon age 13,319–12,961 cal BP recorded, as the oldest age found in the deposit (Fig. 11B, Table 1).

Therefore, we infer that shoreface-connected ridges initially formed oblique to the coast, in NW–SE direction, because the area was much more exposed to storm events coming from the south. Subsequently, after a period where bioturbation was predominant (coinciding with high-amplitude reflectors radiocarbon dated 9885–11,180 cal BP, Table 1), which indicates reduced rates of deposition, the sand ridges were superimposed by 2 m high dunes, which fully grew after the Younger Dryas (Figs. 10D, 14), as suggested by the steeper dip of

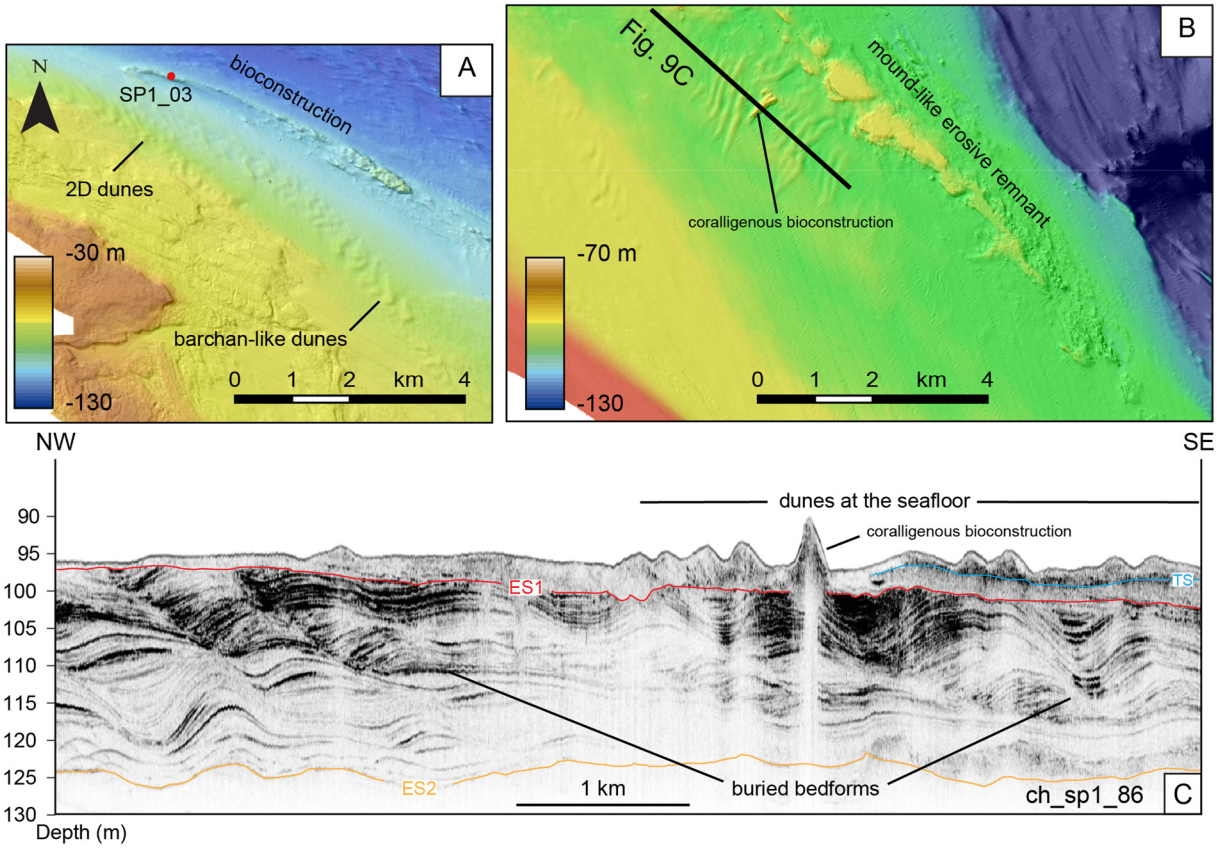

Fig. 9. 5 m resolution DTM of the bathymetry of the topography-constrained large dunes A: off Brindisi and B: north of Cape Otranto. C. CHIRP seismic profile across the dunes of B, where the orientation of crest axes shows consistent NW migration of the buried bedforms deposited between ES2 and ES1.

reflections on top of the high-amplitude reflectors (Fig. 10C).

However, the depth/height ratio rule must be taken with reservation, because water depth is not the only control factor in defining dune size, especially in deep waters, where dune growth is not limited by water depth (Flemming, 2000). Dunes continue to grow in response to increases in mean flow velocity until the critical suspension threshold for a given grain size is reached, because the resulting scaling factor is indeed function of the grain size and coarser sediments normally have lower height/depth ratios compared to finer sediments (Flemming, 2000). This is in agreement with the observation that the Otranto dunes have heights between 2 and 6 m, with higher heights prevailing in the southern sector and corresponding to the inferred shoreface-connected ridges. Six metre high dunes are comprised of shallow sands (D_{50} = 0.21 mm) on their crests (superimposed dunes) and show height/depth ratio = 0.06. On the contrary dunes having coarser grain sizes (D_{50} = 0.4 mm) do not exceed 2 m in height and do not have superimposed bedforms.

In the western Mediterranean, coralligenous bioconstructions formed mostly in the early Holocene (from about 8.5 kyr BP) at paleodepths not > 10–15 m, in low to moderate hydrodynamic conditions (Lo Iacono et al., 2018). Thus, in the study area, dunes located along the edges of bathymetric reliefs, represented by coralligenous bioconstructions (Fig. 9A), likely formed during the last phase of marine transgression and fully developed during the subsequent high stand (Fig. 14), with prevailing southward direct flows as the only ubiquitous sediment-transport mechanism acting in the area.

6.3. Longitudinal bedforms as indicators of persistent unidirectional flows

Erosional and longitudinal depositional features developed in the most sediment-starved sector of the shelf (Fig. 3) and are represented by deep-rooted scours elongated parallel to the shelf edge, comet marks and sand shadows, longitudinal furrows (Fig. 7A). The geometry and dimensions of the erosive features (*i.e.* the erosive tail of a comet mark) are controlled by the size of the obstacle and the intensity and duration of the currents (Werner et al., 1980). In the study area, the modest length of the erosive tails is compatible with persistent unidirectional currents. Furthermore, under the action of such currents, the erosive tails may tend to a quasi-infinite length, forming structures similar to sand ribbons (Kuijpers et al., 2002). In the study area, we observe deposition prevailing over erosion in the up-current side of the obstacles, where sand ribbons or sand shadows form (Fig. 7B). Sand shadows (*sensu* Flemming, 1980) are in fact longitudinal bedforms and form tongue-like sand accumulations attached to the downstream side of obstacles in the flow-path, in areas of low sediment availability. They represent reliable indicators of sand transport directions and hence near-bottom flow direction. Low, rocky outcrops appear to be particularly well suited for the formation of sand shadows in the rear of the obstacles (Flemming, 1980). The typical obstacles found on the SAM shelf are 7 m high, with few reaching up to 10 m (Fig. 7C), offering good conditions for the formation of sand shadows.

When obstacles are absent or very small and the shelf becomes even more sediment-starved, sand streamers and large scours progressively substitute sand ribbons towards the shelf edge (Fig. 7A). This lateral partitioning between sand streamers and scours normally indicates a progressive seaward increase in current velocity (Flemming, 1980). Numerical modelling experiments show NAdDW current speed peaking above 0.70 m s^{-1} at the shelf edge (Bonaldo et al., 2016), suggesting that the erosional features, in this sector of the SAM shelf, may indeed have been shaped by unidirectional flows over a prolonged time, virtually encompassing the last post-glacial sea level rise. Numerous studies, from direct measurements and laboratory flume experiments, indicate that near-bottom current speed in the order of 0.25–0.50 m s^{-1} and 0.6–0.9 m s^{-1} can generate respectively sand shadows and sand

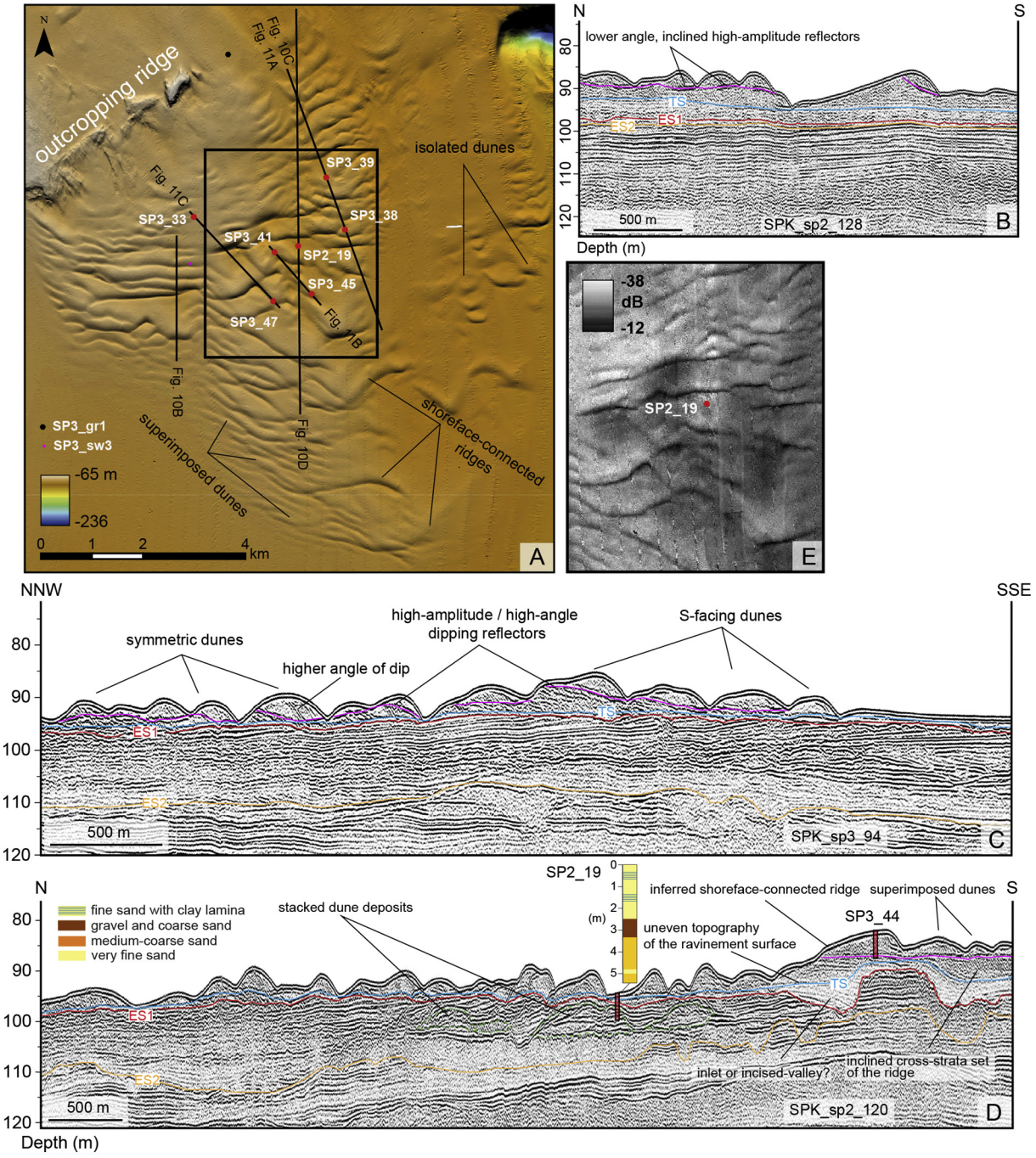

Fig. 10. A. Bathymetry of the Cape Otranto dunes, with location of the seismic profiles and vibrocoring samples (red dots) presented in Figs. 10B, D and 11. B. Sparker seismic profile SPK_sp3_128, N-S oriented across the western sector of the field where linear *E*-W elongated dunes are present. C. Sparker seismic profile SPK_sp3_94 in the northeastern sector of the dune field, documents symmetric dunes, passing to asymmetric south-facing dunes southward. D. Sparker seismic profile SPK_sp2_120, N-S oriented across much of the dune field, showing pits and depressions on the ravinement surface. E. Seafloor backscatter of the dunes sector highlighted by the black rectangle in Fig. 10A. (For interpretation of the references to colour in this figure legend, the reader is referred to the web version of this article.)

dunes (Kuijpers and Nielsen, 2016). These values are comparable to bottom currents driven by unidirectional flows in the study area. However, direct physical observation only spans the last few decades, an interval that is likely too short to include major low-recurrence events and to be extended too far in the past.

6.4. *Margin morphology and shelf width as factors enhancing unidirectional flows*

Though the NAdDW alone may not sustain bed load transport, there are some aspects in the local configuration of the seabed, especially the presence of bathymetric reliefs that act as flow restrictions, which might represent predisposing factors for flow acceleration and play a remarkable role in sediment transport dynamics. Coastal headlands (Pingree, 1978) and locations where the shelf widens, together with topographic ridges, can constrain bottom current flows and enhance their velocity, locally favoring the formation of both erosional features and large-scale bedforms (Barrie et al., 2009; Lo Iacono et al., 2010). Bedforms documenting the action of unidirectional bottom currents are often mapped along the edges of ridges stabilized by bioconstructions

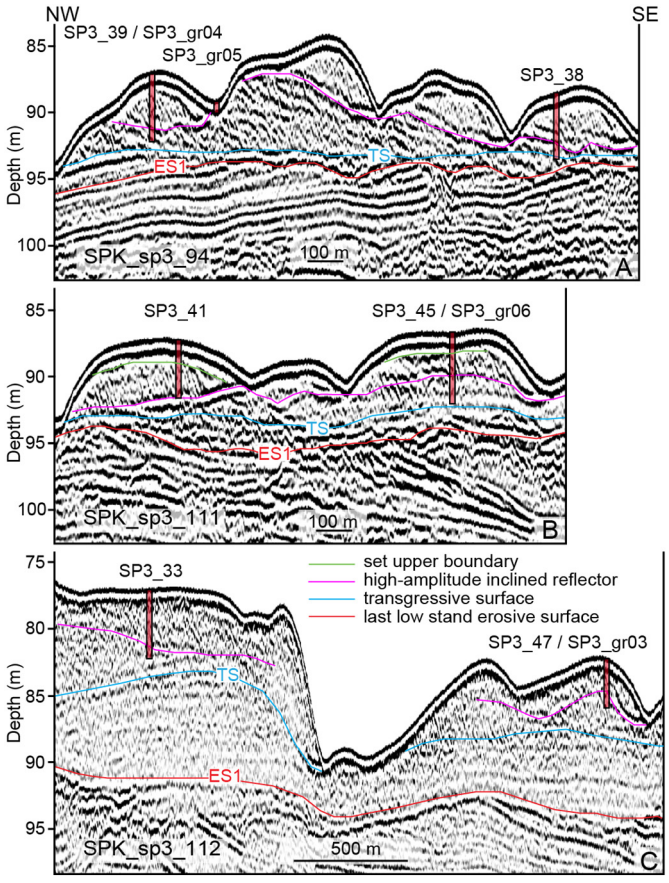

Fig. 11. Close up of the seismic facies of the very large dunes off Cape Otranto. A. Sparker profile SPK_sp3_94, where the high-amplitude inclined seismic facies corresponds to concentrations of shells, dated 10,240–9884 cal BP in core SP3_39 and 11,732–11,180 cal BP in core SP3_38 (Table 2). B. Sparker profile SPK_sp3_111 where the high-amplitude inclined seismic facies corresponds to 9885–9506 cal BP, while the upper boundary of the set of inclined strata was dated at 3392–3036 cal BP (SP3_41, Table 2). C. Sparker profile SPK_sp3_112, where the high-amplitude inclined seismic facies corresponds to radiocarbon dates of 9928–9518 cal BP (SP3_33, Table 2) and 10,563–10,228 cal BP (SP3_47, Table 2). Location of the seismic profiles and sediment cores in Fig. 10A.

and between them, where loose sediments accumulate in the more depressed areas (Lo Iacono et al., 2018). This is what systematically occurs on the SAM shelf, where large fine-medium sand dunes develop landward of erosive remnants (Fig. 9A, B), above the transgressive surface (TS in Fig. 9C). The joint occurrence of comet marks and sand shadows (Fig. 7A) suggests that, beside the availability of sediment, the size and shape of the obstacles are critical factors in determining the shelf morphology. In addition, muddy sediment waves, formed after 5.5 kyr BP, are constrained by topographic steps and develop landward of erosive remnants (Fig. 6A). In particular, they form exclusively where the shelf is rectilinear and narrow (Fig. 3), which might be indicative of some sort of accelerating effect on the WACC geostrophic current flowing southwards along the SAM. The WACC would therefore tend to funnel in this sort of corridor. As a matter of fact, it has been suggested elsewhere that geostrophic currents towards narrower shelves tend to accelerate and to move close inshore (Ramsay et al., 1996). In the study area, muddy sediment waves located seaward of the topographic constraints (field 4 in Fig. 6A) are lower in heights and have lee sides facing eastward, implying that they might be decoupled from the south-directed flow accelerated towards the coast. It can be speculated that the WACC may be reinforced by intensification of the NAdDW during intervals of cooler climatic conditions, such as the Little Ice Age, which resulted in more severe conditions in the North Adriatic (Camuffo et al., 2000). These climate conditions may have enhanced the formation of NAdDW and, concurrently, their ability to impinge on the seafloor morphology. The activity of the NAdDW would remain confined in the outer shelf where giant scours have incised the shelf during the entire last post-glacial phase (Fig. 15, section a).

The sediment drifts elongated parallel to the shelf edge and upper slope (Fig. 3) can be interpreted as shallow-water contourites related to the flow of the NAdDW, based on seismic reflection geometries and terminations (Fig. 8) and direct measurements, which indicate the flow is directed southward along the upper slope (mooring station 4 in Fig. 1). In the study area, contourites extend for > 50 km along the shelf edge and in the outer shelf sectors, immediately downflow of areas of reduced shelf width and inflection of the shelf edge from concave to convex shape (Fig. 3). Here, the acceleration towards the shelf edge of the NAdDW is testified also by the presence of large scours in the outer shelf and moats in the upper slope characterized by orientations compatible with the curvature of the shelf edge (Figs. 7A and 15, section b). The inertial acceleration along a channelized seafloor depression, such as a canyon head, promotes an increase in the current velocity and bottom friction that in turns induces a transport of particles in the Ekman bottom boundary layer, which is forced by the Coriolis effect (Wåhlin and Walin, 2001). In the attempt to adjust to this divergence, the current expels downslope a thin layer of dense fluid (Wåhlin, 2002;

Table 2
Radiocarbon dates of mollusks retrieved in the sediment cores and grabs (SP3_gr, see Fig. 11 for location) and corresponding sediment and acoustic facies. Marine species and genera have been derived from World Register of Marine Species (WoRMS). Available from http://www.marinespecies.org at VLIZ. Accessed 2018–06–11.

Sample	Specimen	Depth (cm bsf)	Conventional Age	Calendar Calibration	Seismic facies	Sediment facies
SP3_gr04	*Atrina fragilis*	seafloor	630 ± 30 BP	260–Post BP 0	Plane-parallel	Muddy sand
SP3_gr06	*Atrina fragilis*	10	1060 ± 30 BP	650–450 cal BP	Plane-parallel	Silty mud
SP3_gr03	*Capulus* sp.	15	1180 ± 30 BP	734–514 cal BP	Plane-parallel	Silty mud
SP3_41	*Capulus* sp.	260	3490 ± 30 BP	3392–3036 cal BP	Set upper boundary	Sand
SP3_41	*Atrina fragilis*	277	6850 ± 30 BP	7408–7136 cal BP	Inclined	Sand
SP3_45	*Atrina fragilis*	325	7210 ± 30 BP	7685–7436 cal BP	Inclined	Sand
SP3_45	*Pecten* sp.	335	9440 ± 30 BP	10,300–9909 cal BP	High-amplitude inclined	Silty sand
SP3_38_	*Pecten* sp.	335	10,460 ± 40 BP	11,732–11,180 cal BP	High-amplitude inclined	Silty sand
SP3_47	*Pecten* sp.	280	9660 ± 30 BP	10,563–10,228 cal BP	High-amplitude inclined	Silty sand
SP3_44	*Mactra* sp.	330	9730 ± 30 BP	10,656–10,277 cal BP	High-amplitude inclined	Silty sand
SP3_44	*Pecten* sp.	310	9800 ± 30 BP	10,755–10,385 cal BP	High-amplitude inclined	Silty sand
SP3_41	*Pecten* sp.	400	9110 ± 30 BP	9885–9506 cal BP	High-amplitude inclined	Silty sand
SP3_39	*Pecten* sp.	230	9400 ± 30 BP	10,240–884 cal BP	High-amplitude inclined	Silty sand
SP3_33	*Mactra* sp.	450	9140 ± 30 BP	9928–9518 cal BP	High-amplitude inclined	Silty sand
SP3_45	*Callista* sp.	380	11,790 ± 40 BP	13,319–12,961 cal BP	Transgressive Surface	Coarse sand

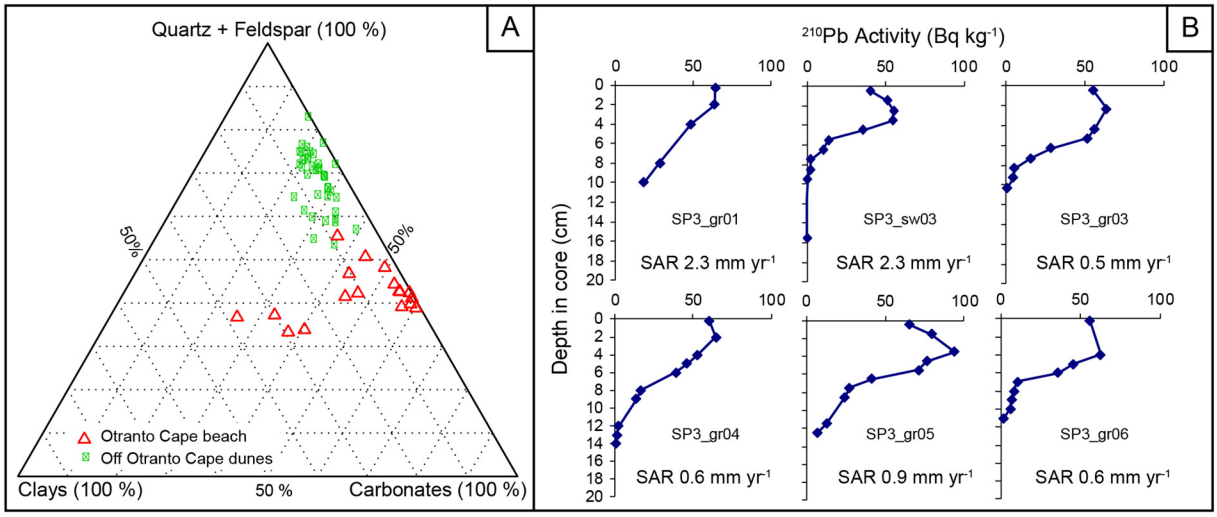

Fig. 12. A. Mineralogic composition of seafloor samples of the dunes off Cape Otranto (green rectangles), compared to modern beach sands (red triangles) of the same area from Ambrosano et al. (1986). The two data sets do not correlate well, suggesting advection from a different compositional province through the action of southward flowing NAdDW. B. Activity profiles of the short-lived ^{210}Pb radionuclide for the last 100 years. Location of the samples in Figs. 10A, 11. (For interpretation of the references to colour in this figure legend, the reader is referred to the web version of this article.)

detrainment in Fig. 16). If we apply such a model to our case study, where moats are elongated parallel to the bathymetric contour, the strata geometry and terminations (Fig. 8A) suggest that such feedback between hydrodynamics and seafloor morphology results not only in a detrainment downslope but also upslope (Fig. 16), controlling the sectors of erosion, deposition and by-pass and the overall asymmetry of the contouritic deposits (Fig. 16). This observation suggests that 3D dynamics of the flow should be included in the models to better represent the interaction of the dense water with the seabed.

Contourite deposition is inhibited in sectors of the margin where the shelf is narrow, the curvature of the shelf edge is subdued and the gradient of the upper slope is higher (as in the Strait of Otranto). This is in agreement with upstream deposition favored around capes, and downstream location of deposits associated with a bottom current flowing over a gentle slope (Falcini et al., 2016).

Furthermore, the coastal morphology and inner shelf bathymetry around capes and headlands may locally accelerate shore-parallel currents (Harrison et al., 2003) and waves (Fig. 2A). Along the SAM shelf there are two areas, which may be undergoing acceleration, around the Gargano Promontory and Cape Otranto (Figs. 1, 15 section c). In both cases, smaller-scale bedforms are suggested to occur superimposed on larger-scale sedimentary features (Figs. 5A, 7B, 10A and D). Indeed, the presence of superimposed bedforms has been often invoked as an evidence for present-day activity (Bassetti et al., 2006; Field et al., 1981; Li and King, 2007) or for storm waves eroding the surface of deep outer shelf sand ridges (Albarracín et al., 2014). In addition, the superimposed bedforms described over the crests of the Manfredonia active sand ridge show barchanoid shapes (Fig. 5A), which are indicative of low sediment-supply and unidirectional flows (Daniell and Hughes, 2007; Todd, 2005), compatible with the path of the NAdDW in that sector of the shelf (Fig. 1). On the contrary, sand ridges which are buried below m-thick muddy sediment in the Gulf of Manfredonia are undergoing degradation in their seafloor relief, therefore can be defined as moribund and may help constrain the actual narrow range of bathymetric contours where the NAdDW circumvents and accelerates around the Gargano Promontory and flows south along the outer shelf (Table 1, Fig. 3).

The sand ridges located in the Strait of Otranto show no interaction with the modern seafloor processes, possibly implying that the NAdDW arrives in the Strait of Otranto with minimum volumes and momentum, and can be considered as relict features (Table 1). At the same time, here the shelf is narrow which does not favor the acceleration of the flow towards the shelf edge, where the sand ridges develop (Fig. 3). SARs based on short-lived radionuclides are low in the Otranto dunes and up to seven-fold higher in adjacent areas (Fig. 12B), suggesting that the mud drape may be occasionally remobilized on the dunes top by

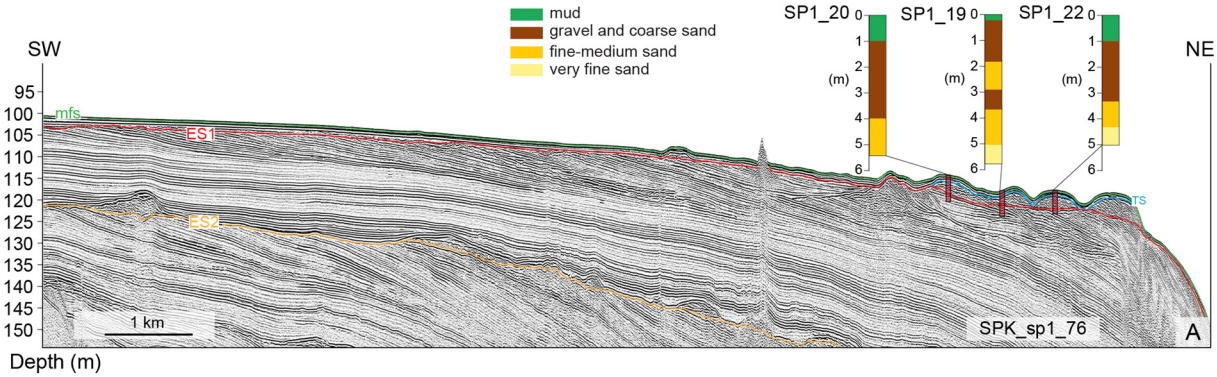

Fig. 13. Seismic sparker profile SPK_SP1_76 (location in Fig. 3) across the sediment starved shelf sector south of Cape Otranto, with location and logs of the cores collected on the linear N-S oriented sand bodies. SP1_22 shows 1 m of mud sealing 4 m of coarse and very coarse sand (D_{50} = 0.5–1.5). Core SP1_19 shows gravel and coarse sand draped by 30 cm of mud. Core SP1_20 is similar to SP1_22 and presents 1 m of mud overlaying coarse and very coarse sand with bivalves. Fine muddy layers are inter-bedded in the massive sands.

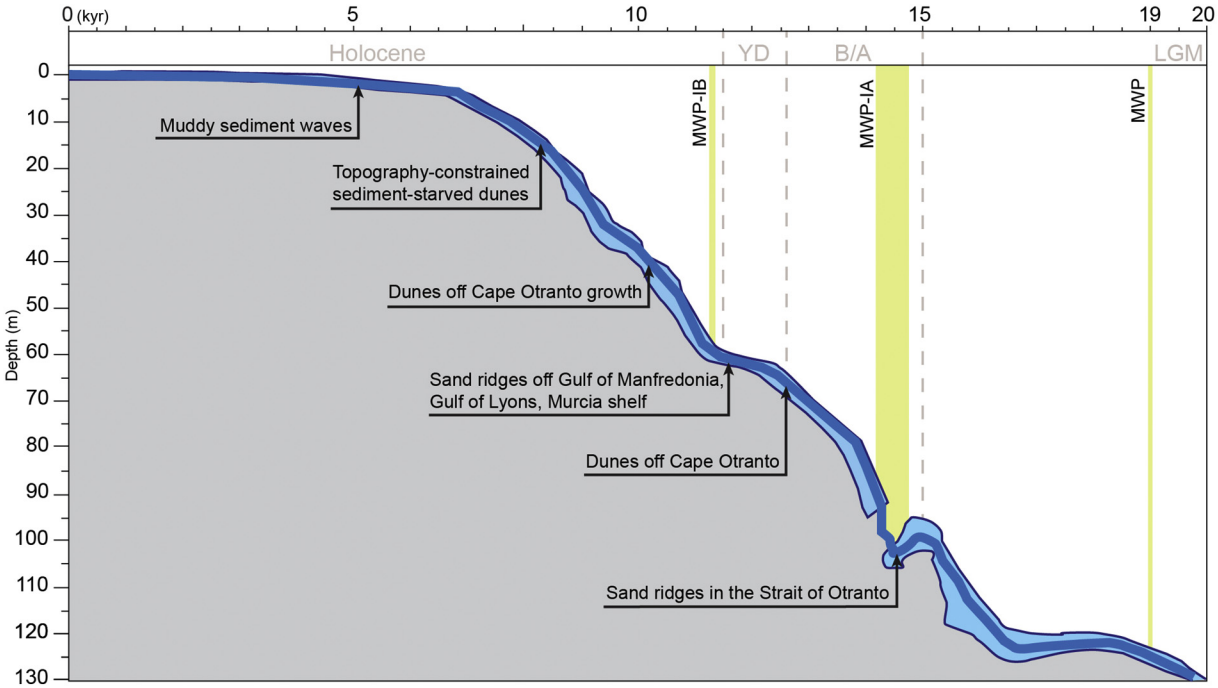

Fig. 14. Sea level curve and major climate events (Lambeck et al., 2014), where the possible ages of formation of the large-scale bedforms on the SAM and in the Mediterranean are indicated. The ice-volume equivalent sea level estimate is accompanied by its 95% probability limiting values (blue shade, from Lambeck et al., 2014). The climate events are: the Last Glacial Maximum (LGM), the Bølling-Allerød warm period (B/A), the Younger Dryas cold period (YD), timing of melting water pulses: MWP-1A and1B. (For interpretation of the references to colour in this figure legend, the reader is referred to the web version of this article.)

localized bottom-current circulation, placing a further constraint on where the NAdDW actually flows, even if at low speed (Fig. 3).

Finally, dune fields appear rather localized in the study area and may rework pre-concentrated sand deposits. Sand concentration down current of Cape Otranto would occur similarly to other Mediterranean continental margins, such as the Murcia shelf, south of Cape Cope Promontory (Durán et al., 2017), as predicted by flow acceleration models around headlands (Jones et al., 2006). This is why only one large field of dunes developed on the SAM shelf, whereas large and very large dunes occur isolated or in small fields elsewhere throughout the entire study area. In addition, the outcropping rocky ridge located to the north of the Otranto dunes (Fig. 10A) may represent a local source of sediment from its progressive dismantling, feeding the growth of these large-scale bedforms, while at the same time acts as a further accelerating factor for the NAdDW in a narrow shelf with a curved shelf edge. While protected and fed from the north by the dismantling

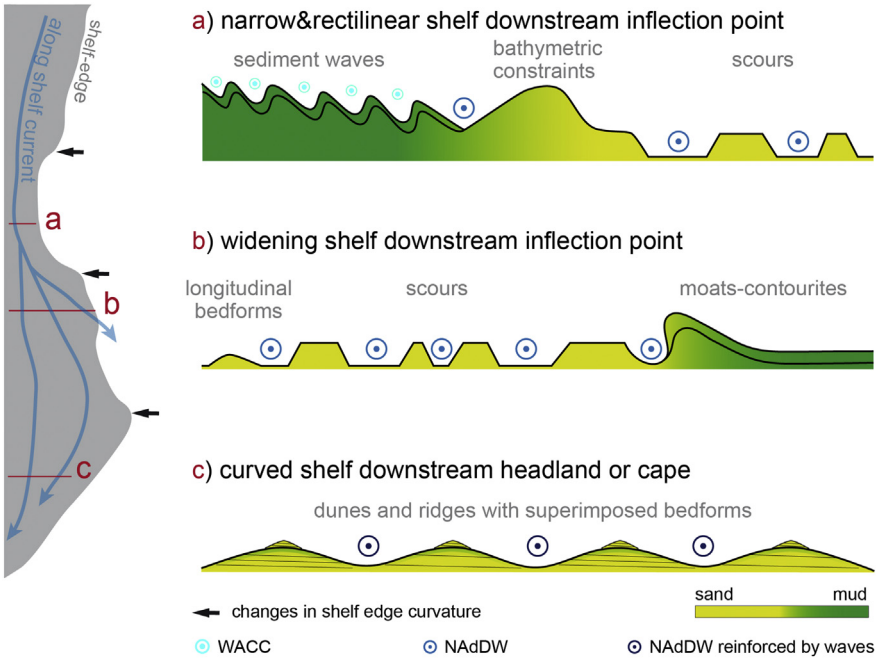

Fig. 15. Schematic transects across the shelf, at three locations characterized by different shelf widths and shelf edge curvatures, representing the sedimentary features formed and preserved from the interaction between seafloor morphology and the path of unidirectional flows flowing north-south.

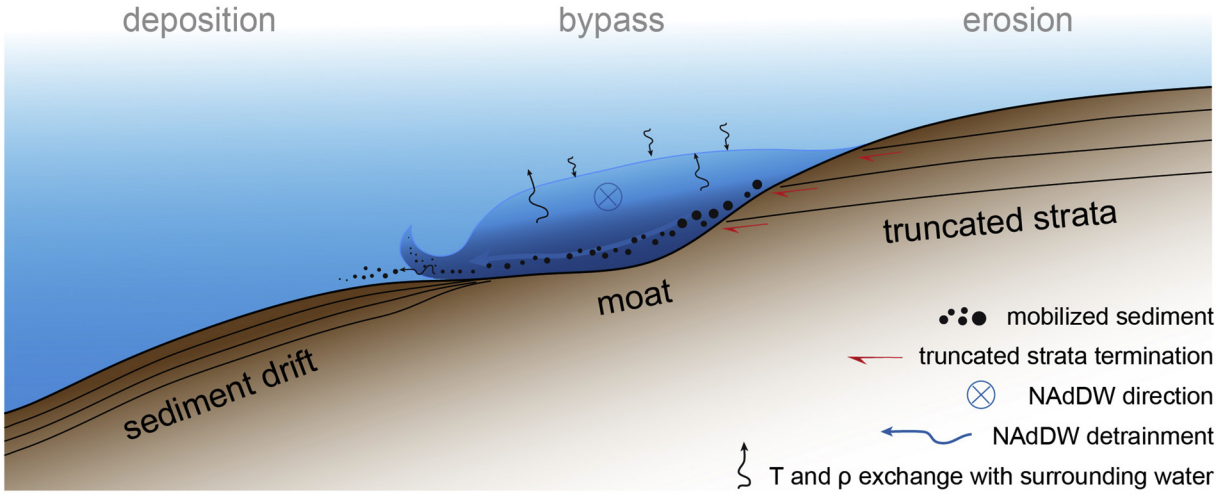

Fig. 16. Anatomy of the NAdDW flowing along a moat, elongated parallel to the shelf edge. The denser water body exchanges temperature and density with the surrounding water column (entrainment) and expels denser water and sediment particles laterally, not only downslope (detrainment).

outcropping ridge, the Otranto dunes are exposed to storm waves from the south (Fig. 2A) and this could possibly explain the observed variation in their asymmetry, with some of the dunes facing N, and different angles in their internal dipping reflectors.

6.5. Resource potential of sandy bedforms

Marine aggregates (sand and gravel) are the main sources for building and land reclamation and partially compensate the decline of inland resources (Bide and Mankelow, 2014), which is also the rationale behind the exploration of the study area in the South Adriatic. Inner continental shelf regions have been the most attractive potential sand sources for beach nourishment for decades as they are shallower and closer to mainland; however since, nearshore sand availability dwindled (Finkl et al., 2007) and the remaining nearshore sand bodies tend to be finer grained and mixed with muddy sediment facies and shell fragments (Williams et al., 2012), prospecting for sand resources is increasingly moving farther offshore. Furthermore, two other aspects have to be considered while exploiting aggregates in shallow waters: one is the preservation of the long-term stability of the coastal equilibrium profile (Suter et al., 1989); secondly the need to avoid the protected *Posidonia oceanica* meadows, especially in the Mediterranean area, and fishing grounds (Lupino and Riccardi, 2001). Outer shelf sand bodies have special economic interest where shelves are sediment-starved and typical large sand reservoir such as those associated to ebb-tidal shoals, shoreface sands and paleoshorelines are limited. Infilled karst depressions have also been explored as potential sand burrowing areas, but in most cases proved unsuitable for beach restoration (Finkl et al., 2007). Therefore, the ability to predict the distribution and accumulation of sand along the outer shelf is becoming crucial for sand resource management.

As said, tidal flows nearshore are extremely sensitive to changes in coastal topography, with resulting acceleration of the flow and local distribution of coastal sediments (Jones et al., 2006). The main process behind asymmetric development of sand ridges around headlands has been disputed for decades. Sand ridges that occur offshore from headlands have been linked to Coriolis acceleration by secondary (Pingree, 1978) or primary flows (Jones et al., 2006) to explain preferential accretion on one side of a headland; however eddy systems with a balance between the centrifugal force and pressure gradient are invoked to explain sand bodies forming at either side (Dyer and Huntley, 1999). In our case study, where the tidal component is negligible, geostrophic unidirectional flows favor asymmetric deposition of sand ridges past headlands and capes (Figs. 3, 15) and this may be used as a predictive tool for sand resource identification in other shelf areas, impacted by unidirectional flows, where baseline information is sparse.

Another key aspect is the compatibility of seafloor sediment character (grain size) and composition (mineral content) of the borrowing sites with the modern beaches, which is crucial for environmental and economical sustainability. Unidirectional currents are responsible for long-shore sediment transport (Fig. 15) resulting in composition of offshore sand resource incompatible with the closest beaches (Fig. 12A). This is an issue that has to be taken into account, especially for beaches with a special landscape value, deriving from their composition.

Finally, shelf sand bodies may also represent oil and gas exploration plays in the rock record. As shelf sand ridges are often encased in muddy sediment seals, they may act as stratigraphic traps providing favourable conditions for hydrocarbons accumulation (Zhu et al., 2008). Tight gas sands refer to low-permeability sandstone reservoirs that produce primarily dry natural gas and are usually associated with heterogeneous grains (*e.g.,* fine grain or muddy sandstones and authigenic cement; Meckel and Thomasson, 2008). In the SAM, lowstand shorefaces normally have large lateral extent and are oriented parallel to bathymetric contours (Figs. 3, 13); sediment facies, in such lowstand bodies, is more heterolithic with fine muddy layers inter-bedded in the coarse and very coarse sand (Fig. 13). On the other hand, transgressive sand bodies have smaller extent of just a few kilometres and variable orientation in respect to the regional bathymetric contours (Figs. 3, 10). These evidences suggest different lateral and horizontal reservoir heterogeneity according to the origin of the sand bodies, with lowstand shorefaces representing preferential target as analogues for hydrocarbon exploration.

7. Conclusions

Unidirectional flows in the Adriatic are related to the geostrophic dynamic of dense shelf waters known to form in wintertime on the shallow North Adriatic shelf, with large inter-decadal variability. South of a slope area impacted by the cascading of dense shelf water, new data across the SW Adriatic Margin (SAM) shelf and upper slope reveal an extensive, over 200 km, area characterized by flute-shaped scours, furrows and comet-marks, accompanied by patches of longitudinal bedforms, muddy sediment waves, sand ridges and very large dunes, that show consistent orientation compatible with southward directed flows, parallel to the coast. At the shelf edge, the area is rimmed by shallow-water muddy contourites and associated contour-parallel moats.

Based on regional reflection seismic and chronological correlations, the lower bounding surface of few shelf bedforms is the surface of subaerial exposure of the area during the Last Glacial Maximum (ES1), while younger bedforms formed after the Younger Dryas cold reversal during the post glacial sea level rise. While glacioeustatic oscillations define the water depth at which sand deposits formed, it is indeed the oceanographic regime that controls their preservation and modification through prolonged time intervals. A key factor is the exact location of unidirectional bottom currents, associated to the flow of dense shelf waters, which guide the cessation or continuation of dune-forming processes and contribute to the erosive sculpting of the shelf and localized sand bodies.

The intensity of the southward flows is intertwined with the local configuration of the seabed, represented by morphological constraints, changes in the curvature of the shelf edge and the interaction with storm waves. In particular:

1. Linear narrow shelf sectors favor the acceleration of unidirectional flows closer inshore and sustain the preservation of older sand dunes and the formation of muddy sediment waves landward of bathymetric constraints (ridges). Seaward of topographic constraints the sole action of dense shelf waters sustains the widespread erosion of the shelf and the presence of large scours.
2. Outward curved and widening shelves, associated with documented acceleration of the flow velocities towards the shelf edge, determine a lateral partitioning between depositional longitudinal bedforms more inshore and erosional features towards the shelf edge and favor the deposition of contourite drifts in the outer shelf and upper slope.
3. Around and downstream of headlands and capes, the acceleration of unidirectional flows combined with enhanced wave activity cause the formation of superimposed smaller-scale barchanoid bedforms, which are indicative of their activity in present-day hydrodynamic conditions.

This finding suggests the importance of the characterization of shelf parameters such shelf width and shelf edge curvature, as good indicators for the prediction of sand bodies, which are potentially exploitable. These conclusions may have also implications for understanding the preservation potential of low stand and transgressive sand bodies in the stratigraphic record as hydrocarbon reservoirs.

Acknowledgments

This study was made possible by the funding provided in 2015–2017 by the Basin Authority of the Apulia Region within the frame of the call for tender “P.O.R. PUGLIA 2000–2006 — FESR” aimed at identifying potential marine sand borrowing areas for combating coastal erosion through beach replenishment actions. Domenico Denora and Nicola Palumbo are warmly recalled for their collaborative efforts in making the project possible. The Authors wish to thank all the researchers, crews' members and students who contributed to the acquisition of data on board several cruises and the analysis of the sediment cores in the laboratories. Listing all of them would not be possible, however MR especially wish to thank Francesco Falese and Chiara Adami for the opening and preliminary sampling of the sediment cores in the laboratories of University La Sapienza, Rome. Sonia Albertazzi carried out the short-lived radionuclides analysis. Leonardo Langone kindly provided suggestions for SAR estimates. Alessandra Mercorella processed a preliminary version of the seafloor backscatter mosaic provided in Fig. 10E. Comments from Katrien Van Landeghem, Guest Editor Veerle Huvenne and an anonymous reviewer were appreciated and greatly improved the organization and readability of the paper.

Data availability

The multibeam datasets related to this article can be found at the EMODnet Bathymetry portal http://www.emodnet-bathymetry.eu/, which is operated and developed by a European partnership, comprising the SeaDataNet consortium. The seismic and core data required to reproduce these findings cannot be shared at this time as the data also forms part of an ongoing study.

References

Albarracín, S., Alcántara-Carrió, J., Montoya-Montes, I., Fontán-Bouzas, Á., Somoza, L., Amos, C.L., Salgado, J.R., 2014. Relict sand waves in the continental shelf of the Gulf of Valencia (Western Mediterranean). J. Sea Res. 93, 33–46. https://doi.org/10.1016/j.seares.2013.12.014.

Ambrosano, E., Ferretti, O., Falcinelli, F., 1986. Tipologia geomorfologica costiera e caratterizzazione mineralogica dei sedimenti di spiaggia del litorale pugliese. In: Indagine Ambientale del Sistema Marino Costiero della Regione Puglia. Elementi per La Definizione Del Piano Delle Coste ENEA, Roma, pp. 55–76.

Amorosi, A., Maselli, V., Trincardi, F., 2016. Onshore to offshore anatomy of a late Quaternary source-to-sink system (Po Plain-Adriatic Sea, Italy). Earth Sci. Rev. 153, 212–237. https://doi.org/10.1016/j.earscirev.2015.10.010.

Artegiani, A., Bregant, D., Paschini, E., Pinardi, N., Raicich, F., Russo, A., 1997. The Adriatic Sea general circulation. Part I: air–sea interactions and water mass structure. J. Phys. Oceanogr. 27, 1492–1514. https://doi.org/10.1175/1520-0485(1997)027<1492:TASGCP>2.0.CO;2.

Barrie, J.V., Conway, K.W., Picard, K., Greene, H.G., 2009. Large-scale sedimentary bedforms and sediment dynamics on a glaciated tectonic continental shelf: examples from the Pacific margin of Canada. Cont. Shelf Res. 29, 796–806. https://doi.org/10.1016/j.csr.2008.12.007.

Bassetti, M.A., Jouet, G., Dufois, F., Berné, S., Rabineau, M., Taviani, M., 2006. Sand bodies at the shelf edge in the Gulf of Lions (Western Mediterranean): Deglacial history and modern processes. Mar. Geol. 234, 93–109. https://doi.org/10.1016/j.margeo.2006.09.010.

Benetazzo, A., Bergamasco, A., Bonaldo, D., Falcieri, F.M., Sclavo, M., Langone, L., Carniel, S., 2014. Response of the Adriatic Sea to an intense cold air outbreak: dense water dynamics and wave-induced transport. Prog. Oceanogr. 128, 115–138. https://doi.org/10.1016/j.pocean.2014.08.015.

Berné, S., Lericolais, G., Marsset, T., Bourillet, J.F., De Batist, M., 1998. Erosional offshore sand ridges and lowstand shorefaces; examples from tide- and wave-dominated environments of France. J. Sediment. Res. 68, 540–555. https://doi.org/10.2110/jsr.68.540.

Berné, S., Vagner, P., Guichard, F., Lericolais, G., Liu, Z., Trentesaux, A., Yin, P., Yi, H. Il, 2002. Pleistocene forced regressions and tidal sand ridges in the East China Sea. Mar. Geol. 188, 293–315. https://doi.org/10.1016/S0025-3227(02)00446-2.

Bide, T., Mankelow, J., 2014. Mapping marine sand and gravel. Planet Earth 14–15.

Bignami, F., Salusti, E., Schiarini, S., 1990. Observations on a bottom vein of dense water in the southern Adriatic and Ionian seas. J. Geophys. Res. 95, 7249. https://doi.org/10.1029/JC095iC05p07249.

Bonaldo, D., Benetazzo, A., Bergamasco, A., Campiani, E., Foglini, F., Sclavo, M., Trincardi, F., Carniel, S., 2016. Interactions among Adriatic continental margin morphology, deep circulation and bedform patterns. Mar. Geol. 375, 82–98. https://doi.org/10.1016/j.margeo.2015.09.012.

Calvete, D., Walgreen, M., de Swarf, H.E., Falqués, A., 2001. A model for sand ridges on the shelf: effect of tidal and steady currents. J. Geophys. Res. C Ocean. 106, 9311–9325. https://doi.org/10.1029/2001JC900001.

Camuffo, D., Secco, C., Brimblecombe, P., Martin-Vide, J., 2000. Sea storms in the Adriatic Sea and the Western Mediterranean during the last millennium. Clim. Chang. 46, 209–223. https://doi.org/10.1023/A:1005607103766.

Canals, M., Puig, P., De Madron, X.D., Heussner, S., Palanques, A., Fabres, J., 2006. Flushing submarine canyons. Nature 444, 14–17. https://doi.org/10.1038/nature05271.

Carniel, S., Bonaldo, D., Benetazzo, A., Bergamasco, A., Boldrin, A., Falcieri, F.M., Sclavo, M., Trincardi, F., Langone, L., 2016. Off-shelf fluxes across the southern Adriatic margin: factors controlling dense-water-driven transport phenomena. Mar. Geol. 375, 44–63. https://doi.org/10.1016/j.margeo.2015.08.016.

Cattaneo, A., Correggiari, A., Langone, L., Trincardi, F., 2003. The late-Holocene Gargano subaqueous delta, Adriatic shelf: sediment pathways and supply fluctuations. Mar. Geol. 193, 61–91. https://doi.org/10.1016/S0025-3227(02)00614-X.

Cattaneo, A., Correggiari, A., Marsset, T., Thomas, Y., Marsset, B., Trincardi, F., 2004. Seafloor undulation pattern on the Adriatic shelf and comparison to deep-water sediment waves. Mar. Geol. 213, 121–148. https://doi.org/10.1016/j.margeo.2004.10.004.

Cattaneo, A., Trincardi, F., Asioli, A., Correggiari, A., 2007. The Western Adriatic shelf clinoform: energy-limited bottomset. Cont. Shelf Res. 27, 506–525. https://doi.org/10.1016/j.csr.2006.11.013.

Chiggiato, J., Bergamasco, A., Borghini, M., Falcieri, F.M., Falco, P., Langone, L., Miserocchi, S., Russo, A., Schroeder, K., 2016. Dense-water bottom currents in the Southern Adriatic Sea in spring 2012. Mar. Geol. 375, 134–145. https://doi.org/10.1016/j.margeo.2015.09.005.

Correggiari, A., Trincardi, F., Langone, L., Roveri, M., Anonymous, 2001. Styles of failure in late Holocene highstand prodelta wedges on the Adriatic shelf. J. Sediment. Res.

71, 218–236. https://doi.org/10.1306/042800710218.
Cushman-Roisin, B., Naimie, C.E., 2002. A 3D finite-element model of the Adriatic tides. J. Mar. Syst. 37, 279–297. https://doi.org/10.1016/S0924-7963(02)00204-X.
Daniell, J.J., Hughes, M., 2007. The morphology of barchan-shaped sand banks from western Torres Strait, northern Australia. Sediment. Geol. 202, 638–652. https://doi.org/10.1016/j.sedgeo.2007.07.007.
Dominici, R., Donato, P., Basta, P., Romano, G., Delle Rose, M., Tenuta, M., Vacca, C., Verrino, M., De Rosa, R., 2016. Mineralogical and textural characterization of the Alimini beach sands: implication on their provenance and transport processes. Rend. Online Soc. Geol. Ital. 38, 39–42. https://doi.org/10.3301/ROL.2016.12.
Dorman, C.E., Carniel, S., Cavaleri, L., Sclavo, M., Chiggiato, J., Doyle, J., Haack, T., Pullen, J., Grbec, B., Vilibić, I., Janeković, I., Lee, C., Malačič, V., Orlić, M., Paschini, E., Russo, A., Signell, R.P., 2007. February 2003 marine atmospheric conditions and the bora over the northern Adriatic. J. Geophys. Res. 112, C03S03. https://doi.org/10.1029/2005JC003134.
Durán, R., Guillén, J., Rivera, J., Lobo, F.J., Muñoz, A., Fernández-Salas, L.M., Acosta, J., 2017. Formation, evolution and present-day activity of offshore sand ridges on a narrow, tideless continental shelf with limited sediment supply. Mar. Geol. 397, 93–107. https://doi.org/10.1016/j.margeo.2017.11.001.
Dyer, K.R., Huntley, D.A., 1999. The origin, classification and modelling of sand banks and ridges. Cont. Shelf Res. 19, 1285–1330. https://doi.org/10.1016/S0278-4343(99)00028-X.
Edwards, J.H., Harrison, S.E., Locker, S.D., Hine, A.C., Twichell, D.C., 2003. Stratigraphic framework of sediment-starved sand ridges on a mixed siliciclastic/carbonate inner shelf; west-central Florida. Mar. Geol. 200, 195–217. https://doi.org/10.1016/S0025-3227(03)00182-8.
Egbert, G.D., Erofeeva, S.Y., 2002. Efficient inverse modeling of bortropic ocean tides. J. Atmos. Ocean. Technol. 19, 183–204. https://doi.org/10.1175/1520-0426(2002)019<0183:EIMOBO>2.0.CO;2.
Falcini, F., Martorelli, E., Chiocci, F.L., Salusti, E., 2016. A general theory for the effect of local topographic unevenness on contourite deposition around marine capes: an inverse problem applied to the Italian continental margin (Cape Suvero). Mar. Geol. 378, 74–80. https://doi.org/10.1016/j.margeo.2016.01.004.
Field, M.E., Nelson, C.H., Cacchione, D.A., Drake, D.E., 1981. Sand waves on an epicontinental shelf: northern Bering Sea. Mar. Geol. 42, 233–258.
Finkl, C.W., Benedet, L., Andrews, J.L., Suthard, B., Locker, S.D., 2007. Sediment ridges on the west Florida inner continental shelf: sand Resources for Beach Nourishment. J. Coast. Res. 231, 143–159. https://doi.org/10.2112/06A-0014.1.
Flemming, B.W., 1980. Sand transport and bedform patterns on the continental shelf between Durban and Port Elizabeth (southeast African continental margin). Sediment. Geol. 26, 179–205. https://doi.org/10.1016/0037-0738(80)90011-1.
Flemming, B.W., 2000. The role of grain size, water depth and flow velocity as scaling factors controlling the size of subaqueous dunes. In: Marine Sandwave Dynamics, pp. 55–61.
Foglini, F., Campiani, E., Trincardi, F., 2016. The reshaping of the south west Adriatic margin by cascading of dense shelf waters. Mar. Geol. 375, 64–81. https://doi.org/10.1016/j.margeo.2015.08.011.
Frignani, M., Langone, L., 1991. Accumulation rates and 137Cs distribution in sediments off the Po River delta and the Emilia-Romagna coast (northwestern Adriatic Sea, Italy). Cont. Shelf Res. 11, 525–542.
Goff, J.A., Swift, D.J.P., Duncan, C.S., Mayer, L.A., Hughes-Clarke, J., 1999. High-resolution swath sonar investigation of sand ridge, dune and ribbon morphology in the offshore environment of the New Jersey margin. Mar. Geol. 161, 307–337. https://doi.org/10.1016/S0025-3227(99)00073-0.
Guerrero, Q., Guillén, J., Durán, R., Urgeles, R., 2018. Contemporary genesis of sand ridges in a tideless erosional shoreface. Mar. Geol. 395, 219–233. https://doi.org/10.1016/j.margeo.2017.10.002.
Harris, P.T., Brancolini, G., Armand, L., Busetti, M., Beaman, R.J., Giorgetti, G., Presti, M., Trincardi, F., 2001. Continental shelf drift deposit indicates non-steady state Antarctic bottom water production in the Holocene. Mar. Geol. 179, 1–8. https://doi.org/10.1016/S0025-3227(01)00183-9.
Harrison, S.E., Locker, S.D., Hine, A.C., Edwards, J.H., Naar, D.F., Twichell, D.C., Mallinson, D.J., 2003. Sediment-starved sand ridges on a mixed carbonate/siliciclastic inner shelf off west-central Florida. Mar. Geol. 200, 171–194. https://doi.org/10.1016/S0025-3227(03)00182-8.
Hernández-Molina, F.J., Soto, M., Piola, A.R., Tomasini, J., Preu, B., Thompson, P., Badalini, G., Creaser, A., Violante, R.A., Morales, E., Paterlini, M., De Santa Ana, H., 2016. A contourite depositional system along the Uruguayan continental margin: sedimentary, oceanographic and paleoceanographic implications. Mar. Geol. 378, 333–349. https://doi.org/10.1016/j.margeo.2015.10.008.
Jones, O.P., Simons, R.R., Jones, E.J.W., Harris, J.M., 2006. Influence of seabed slope and Coriolis effects on the development of sandbanks near headlands. J. Geophys. Res. Oceans 111, 1–23. https://doi.org/10.1029/2005JC002944.
Knaapen, M.A.F., 2005. Sandwave migration predictor based on shape information. J. Geophys. Res. Earth Surf. 110, 1–9. https://doi.org/10.1029/2004JF000195.
Kovačević, V., Gačić, M., Poulain, P.M., 1999. Eulerian current measurements in the Strait of Otranto and in the Southern Adriatic. J. Mar. Syst. 20, 255–278. https://doi.org/10.1016/S0924-7963(98)00086-4.
Kubo, Y., Soh, W., Machiyama, H., Tokuyama, H., 2004. Bedforms produced by the Kuroshio current passing over the northern Izu Ridge. Geo-Mar. Lett. 24, 1–7. https://doi.org/10.1007/s00367-003-0134-1.
Kuijpers, A., Nielsen, T., 2016. Near-bottom current speed maxima in North Atlantic contourite environments inferred from current-induced bedforms and other seabed evidence. Mar. Geol. 378, 230–236. https://doi.org/10.1016/j.margeo.2015.11.003.
Kuijpers, A., Hansen, B., Hühnerbach, V., Larsen, B., Nielsen, T., Werner, F., 2002. Norwegian Sea overflow through the Faroe-Shetland gateway as documented by its bedforms. Mar. Geol. 188, 147–164. https://doi.org/10.1016/S0025-3227(02)00279-7.
Lambeck, K., Rouby, H., Purcell, A., Sun, Y., Sambridge, M., 2014. Sea level and global ice volumes from the Last Glacial Maximum to the Holocene. Proc. Natl. Acad. Sci. U. S. A. 111, 15296–15303. https://doi.org/10.1073/pnas.1411762111.
Langone, L., Conese, I., Miserocchi, S., Boldrin, A., Bonaldo, D., Carniel, S., Chiggiato, J., Turchetto, M., Borghini, M., Tesi, T., 2016. Dynamics of particles along the western margin of the Southern Adriatic: processes involved in transferring particulate matter to the deep basin. Mar. Geol. 375, 28–43. https://doi.org/10.1016/j.margeo.2015.09.004.
Li, M.Z., King, E.L., 2007. Multibeam bathymetric investigations of the morphology of sand ridges and associated bedforms and their relation to storm processes, Sable Island Bank, Scotian Shelf. Mar. Geol. 243, 200–228. https://doi.org/10.1016/j.margeo.2007.05.004.
Lo Iacono, C., Guillén, J., Puig, P., Ribó, M., Ballesteros, M., Palanques, A., Lí Farrán, M., Acosta, J., 2010. Large-scale bedforms along a tideless outer shelf setting in the western Mediterranean. Cont. Shelf Res. 30, 1802–1813. https://doi.org/10.1016/j.csr.2010.08.005.
Lo Iacono, C., Savini, A., Basso, D., 2018. Cold-water carbonate bioconstructions. In: Micallef, A., Savini, A., Krastel, S. (Eds.), Submarine Geomorphology. Springer Geology, pp. 425–455. https://doi.org/10.1007/978-3-319-57852-1.
Lupino, P., Riccardi, C., 2001. Utilisation of marine sand for beach nourishment in the western Mediterranean. In: Özhan, E. (Ed.), Proceedings of the Fifth International Conference on the Mediterranean Coastal Environment. Middle East Technical University, Ankara, pp. 1347–1358.
Madsen, O.S., Wood, W., 2002. Sediment transport outside the Surf Zone. In: Vincent, L., Demirbilek, Z. (Eds.), Coastal Engineering Manual. U.S. Army Corps of Engineers, Washington, DC, pp. 72.
McBride, R.A., Moslow, T.F., 1991. Origin, evolution, and distribution of shoreface sand ridges, Atlantic inner shelf, U.S.A. Mar. Geol. 97, 57–85. https://doi.org/10.1016/0025-3227(91)90019-Z.
Meckel, L.D., Thomasson, M.R., 2008. Pervasive tight-gas sandstone reservoirs: an overview. In: Cumella, S.P., Shanley, K.W., Camp, W.K. (Eds.), Understanding, Exploring, and Developing Tight-Gas Sands—2005 Vail Hedberg Conference. AAPG Hedberg Series, vol. 3. pp. 13–27. https://doi.org/10.1306/13131047H33321.
Mihanović, H., Vilibić, I., Carniel, S., Tudor, M., Russo, A., Bergamasco, A., Bubić, N., Ljubešić, Z., Viličić, D., Boldrin, A., Malačič, V., Celio, M., Comici, C., Raicich, F., 2013. Exceptional dense water formation on the Adriatic shelf in the winter of 2012. Ocean Sci. 9, 561–572. https://doi.org/10.5194/os-9-561-2013.
Nnafie, A., de Swart, H.E., Calvete, D., Garnier, R., 2014. Effects of sea level rise on the formation and drowning of shoreface-connected sand ridges, a model study. Cont. Shelf Res. 80, 32–48. https://doi.org/10.1016/j.csr.2014.02.017.
Park, S.C., Han, H.S., Yoo, D.G., 2003. Transgressive sand ridges on the mid-shelf of the southern sea of Korea (Korea Strait): Formation and development in high-energy environments. Mar. Geol. 193, 1–18. https://doi.org/10.1016/S0025-3227(02)00611-4.
Pellegrini, C., Maselli, V., Cattaneo, A., Piva, A., Ceregato, A., Trincardi, F., 2015. Anatomy of a compound delta from the post-glacial transgressive record in the Adriatic Sea. Mar. Geol. 362, 43–59. https://doi.org/10.1016/j.margeo.2015.01.010.
Pellegrini, C., Maselli, V., Trincardi, F., 2016. Pliocene–Quaternary contourite depositional system along the south-western Adriatic margin: changes in sedimentary stacking pattern and associated bottom currents. Geo-Mar. Lett. 36, 67–79. https://doi.org/10.1007/s00367-015-0424-4.
Pellegrini, C., Maselli, V., Gamberi, F., Asioli, A., Bohacs, K.M., Drexler, T.M., Trincardi, F., 2017. How to make a 350-m-thick lowstand systems tract in 17,000 years: the Late Pleistocene Po River (Italy) lowstand wedge. Geology 45, 327–330. https://doi.org/10.1130/G38848.1.
Pellegrini, C., Asioli, A., Bohacs, K.M., Drexler, T.M., Feldman, H.R., Sweet, M.L., Maselli, V., Rovere, M., Gamberi, F., Valle, G.D., Trincardi, F., 2018. The late Pleistocene Po River lowstand wedge in the Adriatic Sea: controls on architecture variability and sediment partitioning. Mar. Pet. Geol. 96, 16–50. https://doi.org/10.1016/j.marpetgeo.2018.03.002.
Pingree, R.D., 1978. The formation of the shambles and other banks by tidal stirring of the seas. J. Mar. Biol. Assoc. U. K. 58, 211–226. https://doi.org/10.1017/S0025315400024504.
Piscopia, R., Franco, L., Corsini, S., Inghilesi, R., 2004. L'Atlante delle onde nei mari italiani - Italian Wave Atlas [WWW Document]. Univ. Roma TRE - APAT. http://www.isprambiente.gov.it/it/pubblicazioni/rapporti/atlante-delle-onde-nei-mari-italiani.
Piva, A., Asioli, A., Trincardi, F., Schneider, R.R., Vigliotti, L., 2008. Late-Holocene climate variability in the Adriatic Sea (Central Mediterranean). The Holocene 18, 153–167. https://doi.org/10.1177/0959683607085606.
Poulain, P.M., 2001. Adriatic Sea surface circulation as derived from drifter data between 1990 and 1999. J. Mar. Syst. 29, 3–32. https://doi.org/10.1016/S0924-7963(01)00007-0.
Ramsay, P.J., Smith, A.M., Mason, T.R., 1996. Geostrophic sand ridge, dune fields and associated bedforms from the Northern KwaZulu-Natal shelf, south-east Africa. Sedimentology 43, 407–419. https://doi.org/10.1046/j.1365-3091.1996.d01-17.x.
Ridente, D., Trincardi, F., 2002. Eustatic and tectonic control on deposition and lateral variability of quaternary regressive sequences in the Adriatic basin (Italy). Mar. Geol. 184, 273–293. https://doi.org/10.1016/S0025-3227(01)00296-1.
Siddall, M., Rohling, E., Almogi-Labin, A., Hemleben, C., Meischner, D., Schmelzer, I., Smeed, D., 2003. Sea-level fluctuations during the last glacial cycle. Nature 423, 853–858. https://doi.org/10.1038/nature01687.1.
Signell, R.P., Chiggiato, J., Horstmann, J., Doyle, J.D., Pullen, J., Askari, F., 2010. High-resolution mapping of Bora winds in the northern Adriatic Sea using synthetic

aperture radar. J. Geophys. Res. Oceans 115, C04020. https://doi.org/10.1029/2009JC005524.
Snedden, J.W., Tillman, R.W., Culver, S.J., 2011. Genesis and evolution of a mid-shelf, storm-built sand ridge, New Jersey continental shelf, U.S.A. J. Sediment. Res. 81, 534–552. https://doi.org/10.2110/jsr.2011.26.
Suter, J.R., Mossa, J., Penland, S., 1989. Preliminary assessments of the occurrence and effects of utilization of sand and aggregate resources of the Louisiana inner shelf. Mar. Geol. 90, 31–37. https://doi.org/10.1016/0025-3227(89)90111-4.
Swift, D.J.P., Stanley, D.J., Curray, J.R., 1971. Relict sediments on continental shelves: a reconsideration. J. Geol. 79, 322–346.
Swift, D.J.P., Parker, G., Lanfredi, N.W., Perillo, G., Figge, K., 1978. Shoreface-connected sand ridges on American and European shelves: a comparison. Estuar. Coast. Mar. Sci. 7, 257–273. https://doi.org/10.1016/0302-3524(78)90109-3.
Todd, B.J., 2005. Morphology and composition of submarine barchan dunes on the Scotian Shelf, Canadian Atlantic margin. Geomorphology 67, 487–500. https://doi.org/10.1016/j.geomorph.2004.11.016.
Trincardi, F., Correggiari, A., 2000. Quaternary forced regression deposits in the Adriatic basin and the record of composite sea-level cycles. Geol. Soc. Lond. Spec. Publ. 172, 245–269. https://doi.org/10.1144/GSL.SP.2000.172.01.12.
Trincardi, F., Correggiari, A., Roveri, M., 1994. Late Quaternary transgressive erosion and deposition in a modern epicontinental shelf: the Adriatic semienclosed basin. Geo-Mar. Lett. 14, 41–51. https://doi.org/10.1007/BF01204470.
Trincardi, F., Foglini, F., Verdicchio, G., Asioli, A., Correggiari, A., Minisini, D., Piva, A., Remia, A., Ridente, D., Taviani, M., 2007. The impact of cascading currents on the Bari Canyon System, SW-Adriatic margin (Central Mediterranean). Mar. Geol. 246, 208–230. https://doi.org/10.1016/j.margeo.2007.01.013.
Turchetto, M., Boldrin, A., Langone, L., Miserocchi, S., Tesi, T., Foglini, F., 2007. Particle transport in the Bari Canyon (southern Adriatic Sea). Mar. Geol. 246, 231–247. https://doi.org/10.1016/j.margeo.2007.02.007.
Ursella, L., Kovačević, V., Gačić, M., 2014. Tidal variability of the motion in the Strait of Otranto. Ocean Sci. 10, 49–67. https://doi.org/10.5194/os-10-49-2014.
Van Landeghem, K.J.J., Uehara, K., Wheeler, A.J., Mitchell, N.C., Scourse, J.D., 2009. Post-glacial sediment dynamics in the Irish Sea and sediment wave morphology: Data-model comparisons. Cont. Shelf Res. 29, 1723–1736. https://doi.org/10.1016/j.csr.2009.05.014.
Van Landeghem, K.J.J., Baas, J.H., Mitchell, N.C., Wilcockson, D., Wheeler, A.J., 2012. Reversed sediment wave migration in the Irish Sea, NW Europe: a reappraisal of the validity of geometry-based predictive modelling and assumptions. Mar. Geol. 295–298, 95–112. https://doi.org/10.1016/j.margeo.2011.12.004.
Verdicchio, G., Trincardi, F., 2008. Mediterranean shelf-edge muddy contourites: examples from the Gela and South Adriatic basins. Geo-Mar. Lett. 28, 137–151. https://doi.org/10.1007/s00367-007-0096-9.
Verdicchio, G., Trincardi, F., Asioli, A., 2007. Mediterranean bottom-current deposits: An example from the Southwestern Adriatic margin. In: Viana, A.R., Rebesco, M. (Eds.), Economic and Palaeoceanographic Significance of Contourite Deposits. Geological Society, London, pp. 199–224. https://doi.org/10.1144/gsl.sp.2007.276.01.10.
Viana, A.R., Almeida, W., Nunes, M.C.V., Bulhões, E.M., 2007. The economic importance of contourites. Geol. Soc. Lond. Spec. Publ. 276, 1–23. https://doi.org/10.1144/GSL.SP.2007.276.01.01.
Vilibić, I., Supić, N., 2005. Dense water generation on a shelf: the case of the Adriatic Sea. Ocean Dyn. 55, 403–415. https://doi.org/10.1007/s10236-005-0030-5.
Wåhlin, A.K., 2002. Topographic steering of dense currents with application to submarine canyons. Deep-Sea Res. I Oceanogr. Res. Pap. 49, 305–320. https://doi.org/10.1016/S0967-0637(01)00058-9.
Wåhlin, A.K., Walin, G., 2001. Downward migration of dense bottom currents. Environ. Fluid Mech. 1, 257–279. https://doi.org/10.1023/A:1011520432200.
Werner, F., Unsöld, G., Koopmann, B., Stefanon, A., 1980. Field observations and flume experiments on the nature of comet marks. Sediment. Geol. 26, 233–262. https://doi.org/10.1016/0037-0738(80)90013-5.
Williams, S.J., Flocks, J., Jenkins, C., Khalil, S., Moya, J., 2012. Offshore sediment character and sand resource assessment of the northern Gulf of Mexico, Florida to Texas. J. Coast. Res. 10060, 30–44. https://doi.org/10.2112/SI.
Yalin, M.S., 1992. River Mechanics. Pergamon Press, Oxford, pp. 219.
Zhu, H., Chen, K., Liu, K., He, S., 2008. A sequence stratigraphic model for reservoir sandbody distribution in the Lower Permian Shanxi Formation in the Ordos Basin, northern China. Mar. Pet. Geol. 25, 731–743. https://doi.org/10.1016/j.marpetgeo.2008.03.007.